

RESEARCH ARTICLE

10.1029/2018JA026094

Key Points:

- Spatial features of low-latitude Pi2s are derived using multisatellite and ground observations
- Characteristics of Pi2s are identical at night and different at day between satellite and ground
- Oscillating FACs and ionospheric currents are the source for nighttime and daytime Pi2s, respectively

Correspondence to:

N. Thomas,
neethal.thomas@isee.nagoya-u.ac.jp

Citation:

Thomas, N., Shiokawa, K., & Vichare, G. (2019). Comprehensive study of low-latitude Pi2 pulsations using observations from multisatellite Swarm mission and global network of ground observatories. *Journal of Geophysical Research: Space Physics*, 124, 1966–1991. <https://doi.org/10.1029/2018JA026094>




Received 13 SEP 2018

Accepted 4 MAR 2019

Accepted article online 9 MAR 2019

Published online 29 MAR 2019

Comprehensive Study of Low-Latitude Pi2 Pulsations Using Observations From Multisatellite Swarm Mission and Global Network of Ground Observatories

Neethal Thomas¹ , Kazuo Shiokawa¹ , and Geeta Vichare² 

¹Institute for Space-Earth Environmental Research, Nagoya University, Nagoya, Japan, ²Indian Institute of Geomagnetism, Navi Mumbai, India

Abstract To understand the spatial features of low-latitude Pi2 (6.6–25 mHz) pulsations, a comprehensive study is carried out for the first time using magnetic field measurements from a global network of low-latitude ground stations (Mlat: $\pm 2^\circ - 51^\circ$) and the Swarm multisatellites located simultaneously at day and night local times. We have investigated 1-year data from 2014 and found 15 Pi2 events with coherent oscillations at satellite and ground. The Pi2 oscillations in the compressional, toroidal, and poloidal components at satellite and H , D , and Z components at ground are investigated by estimating its coherence, amplitude, and cross phase with respect to midnight ground H variations. The analogous pairs of magnetic field components (satellite compressional with ground H and satellite toroidal with ground D) above and below the ionosphere are found to have identical phase during night and opposite phase during day, indicating the magnetospheric and ionospheric sources for nighttime and daytime Pi2s, respectively. During nighttime, Pi2 oscillations identified in the poloidal component are found to oscillate in phase (out of phase) in the Southern (Northern) Hemisphere. At ground, the phase and amplitude of H showed significant change near the dawn terminator, whereas H oscillates mostly in phase with respect to midnight ground H at other local times. The oscillations in D component have phase reversal near midnight, dawn, dusk, and noon meridians with opposite hemispheres having opposite phase. These Pi2 characteristics observed globally at ground and at the topside ionosphere suggest that the sources for nighttime and daytime low-latitude Pi2s are oscillating field-aligned currents and ionospheric currents, respectively.

1. Introduction

Pi2 pulsations are the transient, ultralow frequency (ULF) oscillations of the Earth's magnetic field with periods of 40–150 s and are commonly observed in association with substorm onset (Saito, 1961). During the onset of substorm expansion phase, the near-Earth magnetotail undergoes a sudden change in its physical state from a stretched configuration to a dipolar form (Cummings et al., 1968; Takahashi et al., 1987). This change in the magnetosphere configuration is caused by the formation of the substorm current wedge (SCW), when the cross-tail current gets short circuited to the auroral ionosphere via field-aligned currents, due to the disruption of tail current (McPherron et al., 1973). Pi2 oscillations can be considered as the manifestation of these sudden changes in the state of the magnetosphere during substorm, which can be observed at different radial distances from the Earth's surface (e.g., Shiokawa et al., 1998). The association of Pi2s with substorms makes it important to study, as it serves as an important proxy for understanding the complex electrodynamic processes taking place in the magnetosphere and the coupling process between magnetosphere and ionosphere.

Although Pi2 is a well-observed phenomenon during substorm, its source region in the magnetosphere and its propagation to the ionosphere and to ground is still not completely understood. Different mechanisms have been proposed to explain Pi2 oscillations observed at low-middle latitudes in the nightside. Plasmaspheric cavity mode resonance is one of the popular models proposed for middle-low latitude Pi2s (Keiling et al., 2001; Nose, 2010; Saito & Matsushita, 1968; Sutcliffe & Yumoto, 1991; Yeoman & Orr, 1989; Takahashi et al., 1995; Yumoto et al., 2001), which considers that the source of Pi2 resides inside the inner magnetosphere. Cavity mode is excited by impulsive compressional fast-mode waves, which propagate earthward in

the magnetic equatorial plane from the magnetotail. Inside the plasmasphere, these fast-mode waves get trapped between the inner (ionosphere) and outer (plasmopause) boundaries and establish standing waves, resulting in Pi2 oscillations at middle-low latitudes (Yeoman & Orr, 1989). However, there are several observations that contradict the idea of cavity nature of low-latitude Pi2 oscillation (Nishimura et al., 2012; Osaki et al., 1998).

Pi2 oscillations at low and middle latitudes were also explained using the SCW model, which considers the oscillations of the pair of upward and downward field-aligned currents (FACs). The formation of the SCW can be identified at low-middle latitude ground locations as magnetic bay signatures. These bay signatures observed in the H and D component has specific longitudinal pattern (Clauer & McPherron, 1974). The relationship between the characteristics features of Pi2 oscillations and the magnetic bay signatures at ground was noticed by many researchers (Gelpi et al., 1985; Lester et al., 1983, 1984, 1989; Nishimura et al., 2012; Samson et al., 1985). Lester et al. (1983) identified that the major axis of the polarization ellipse of midlatitude Pi2 is directed toward the center of the current wedge. They showed that the longitudinal pattern of the polarization ellipse of Pi2 oscillation is organized well with the magnetic bay structure of SCW. Later, it was identified by Lester et al. (1989) that the low-latitude Pi2s has polarization pattern identical to that at midlatitudes. Recent studies by Imajo et al. (2015, 2017) clearly indicates the contribution of nightside SCW FACs on the Pi2 oscillations observed near terminators. These studies indicate that the low-middle latitude Pi2s in the nightside are the magnetic field signatures of the oscillating FACs of SCW. As the FACs are carried by the magnetic field lines that have foot points in the auroral ionosphere, the source of Pi2 can be considered to be outside the inner magnetosphere.

Although Pi2 is a predominant phenomenon in the nightside, they are often observed over a wide local time (LT) sector including daytime at low-latitude (Sutcliffe & Yumoto, 1989, 1991) and equatorial-latitude (Stuart & Barszczus, 1980; Sastry et al., 1983; Yanagihara & Shimizu, 1966) ground stations, with daytime Pi2 observed to have nearly identical period and phase with that of nighttime ones. Different mechanisms proposed to explain the daytime Pi2 signatures in conjunction with substorm phenomenon include cavity oscillations and instantaneous transmission of polar electric fields to the dayside ionosphere. Coherent in-phase oscillations in the H component at day and night ground stations with larger amplitudes in the auroral breakup meridian suggested plasmaspheric cavity as a possible mechanism (Nosé et al., 2006; Sutcliffe & Yumoto, 1991) for daytime Pi2s. Shinohara et al. (1997) in their investigation of day and night Pi2 pulsations using ground observations identified the enhancement of daytime Pi2 amplitude at the dip equator. They explained the enhanced amplitude of daytime Pi2 at equatorial latitudes using the instantaneous penetration of polar electric field model proposed by Kikuchi and Araki (1979). According to Shinohara et al. (1997), the electric field associated with Pi2s launched in the polar ionosphere is instantaneously transmitted to the dayside low- and equatorial-latitude ionospheres. These electric field modulates the strong ionospheric currents in the enhanced ionospheric conductivity regions near dip equator causing magnetic field perturbations in the Pi2 frequency. The existence of daytime Pi2s oscillations in the topside ionosphere was reported by Han et al. (2004) using Ørsted and Thomas et al. (2015) using Challenging Minisatellite Payload (CHAMP) satellite observations. Their observations that showed antiphase oscillations between compressional component at satellite and H component at ground also indicate that daytime Pi2s are caused by ionospheric currents.

Imajo et al. (2015, 2016) identified that the Pi2 oscillations are polarized to D component during terminator hours and have opposite phase relations in the sunlit and darkside (nightside) of the hemisphere. Their study suggest that terminator Pi2s are caused by the meridional ionospheric currents that are driven by nightside FACs. These observations were later numerically tested and confirmed by Imajo et al. (2017) by estimating the spatial distribution of the ground magnetic field caused by the ionospheric-magnetospheric currents.

Low Earth orbiting (LEO) satellites have been extensively used in the study of different ULF geomagnetic pulsations (e.g., Balasis et al., 2012; Heilig et al., 2007; Jadhav et al., 2001; Sutcliffe & Lühr, 2003; Takahashi et al., 1999; Vellante et al., 2004). With observations from the topside ionosphere, LEO satellites can provide useful insights on the role of ionosphere on these oscillations. A number of ULF studies mostly in the Pc3 frequency range (20–100 mHz) have been reported using the observations from Swarm mission (e.g., Balasis et al., 2015; Heilig & Sutcliffe, 2016; Papadimitriou et al., 2018). However, to the best of authors' knowledge, this is the first report of the observation of Pi2 oscillations made using the Swarm mission.

Till date, Pi2s were mostly investigated using observations from a limited LT sector. The morphology of the global Pi2 oscillations and variations in its characteristic features at different LT are not addressed yet. This is important as it helps in visualizing the spatial features of Pi2 oscillations localized to different LT sectors, which one may miss to observe when studied separately. The present study aims to obtain the spatial features of the low-latitude Pi2 oscillations using a network of longitudinally and latitudinally distributed ground stations from both Northern Hemisphere (NH) and Southern Hemisphere (SH) together with the Swarm satellites simultaneously located at day and night LT sectors. The conjugate observations from the satellite and ground play a crucial role in identifying the wave type responsible for the Pi2 oscillations as different magnetic hydrodynamic waves manifest themselves in different components above the ionosphere. The nighttime Pi2 oscillations investigated using satellite observations were mainly reported in the compressional and poloidal components (Han et al., 2004; Sutcliffe & Lühr, 2003; Sutcliffe & Lühr, 2010; Takahashi et al., 1995; Thomas et al., 2015). The present study reports, for the first time, the identification of coherent Pi2 oscillations in the toroidal components. The toroidal components at satellite are found to have phase identical to that of ground D during night hours. Our observations of Pi2 oscillations in different magnetic field components at satellite and ground suggest that low-latitude Pi2s are the magnetic field signatures of the magnetospheric and ionospheric current system formed during substorms, with SCW FAC responsible for nighttime and ionospheric currents responsible for daytime Pi2s.

The paper is organized as follows. Section 2 describes the satellite and ground data used and the methodology adopted in identifying and analyzing the Pi2 events. Section 3 presents two case studies demonstrating the Pi2 oscillations simultaneously observed at satellite and ground. The statistical studies on the LT variation of the phase and amplitude of Pi2 oscillations at satellite and ground are presented separately in section 4. Section 5 discusses the results with the Pi2 models for day, night, and terminator. Section 6 concludes the findings of the present study.

2. Data and Methodology

To investigate the characteristic features of low-latitude Pi2 pulsations, we utilize simultaneous magnetic field measurements from ground and space. As low-latitude Pi2 pulsations are manifested over a wide range of longitudes during substorm onset, the observations covering different LT sectors are employed in this study.

2.1. Ground Data

Present study utilizes vector magnetic field data from 43 ground stations covering all longitude sectors. The geomagnetic latitude range of the ground stations used is 50° N to 51° S through the equator, with 27 ground stations located in the NH and 16 in the SH. The list of the ground stations and its coordinates are detailed in Table 1. The data used comprise horizontal and radial magnetic field components: H (positive north), D (positive east), and Z (positive down) in geomagnetic coordinates. Magnetic field data in geographical coordinates (X , Y , and Z) are transformed into (H , D , and Z) using annual mean declination values of the ground stations obtained from the IGRF 12 model. The magnetic field data used here include the induction coil magnetometer data with 64-Hz sampling recorded at Shillong (SHL) and fluxgate magnetometer with 1-Hz sampling obtained from all other ground stations. The induction coil data at SHL are downsampled to 1 Hz to maintain the uniformity of data sampling.

2.2. Satellite Data

The space-borne observations of Pi2 signatures are made using fluxgate magnetometers on board European Space Agency's (ESA) Swarm satellites. Swarm, a constellation of three satellites A-Alpha, B-Bravo, and C-Charlie, are launched together on November 2013 into near polar (inclination $\sim 87^\circ$) low Earth orbits. After orbital maneuvering, the satellites achieved its final constellation by April 2014, with Swarm A and C flying side by side at an altitude of ~ 470 km and Swarm B in a longitudinally shifted orbit at an altitude of ~ 530 km. Swarm vector fluxgate magnetometer data with 1-Hz sampling in North East Centre coordinates (magnetic product: MAGX_LR_1B) are used in this study. The residual fields at satellite are obtained by subtracting CHAOS-5 (Finlay et al., 2015) geomagnetic field model from the satellite data. For a given location, CHAOS-5 gives an estimate of the Earth's internal (core and crustal) field, its secular variation and acceleration, and the external field contributions from static magnetospheric currents and time-varying ring currents. The residual fields therefore delineate the magnetic field perturbations resulting from ionospheric and magnetospheric sources. The residual magnetic fields at satellite are then transformed into field-aligned

Table 1
List of Ground Stations

Station name	Station code	Geographic		Geomagnetic	
		Latitude	Longitude	Latitude	Longitude
Alma Ata	AAA	43.18	76.92	34.43	153.22
Addis Ababa	AAE	9.03	38.77	5.33	112.45
Martin de Vivies-Amsterdam Island	AMS	-37.8	77.57	-45.87	145.46
Apia	API	-13.8	188.22	-15.07	263.24
Alice Springs	ASP	-23.76	133.88	-32.26	208.83
Budkov	BDV	49.08	14.02	48.53	97.69
Belsk	BEL	51.84	20.79	50.07	105.2
Boulder	BOU	40.14	254.76	47.91	321.84
Stennis	BSL	30.35	270.36	39.45	340.78
Chambon la Foret	CLF	48.02	2.27	49.49	85.77
Canberra	CNB	-35.32	149.36	-42.09	227.39
Charters Towers	CTA	-20.1	146.3	-27.43	221.61
Cheongyang	CYG	36.37	126.85	26.94	197.49
Port Alfred	CZT	-46.43	51.87	-51.08	114.74
Dalat	DLT	11.94	108.48	2.12	181.0
Ebro	EBR	40.95	0.33	42.94	81.41
Eyrewell	EYR	-43.47	172.39	-46.71	254.09
Fredericksburg	FRD	38.2	282.63	47.72	354.34
Fresno	FRN	37.09	240.28	43.15	306.5
Gingin	GNG	-31.35	115.71	-40.81	189.34
Guam	GUA	13.59	144.87	5.7	216.42
Hermanus	HER	-34.43	19.23	-33.99	85.15
Honolulu	HON	21.32	202	21.64	270.71
Isla de Pascua Mataverí (Easter Island)	IPM	-27.2	250.58	-19.12	325.55
Kakioka	KAK	36.23	140.18	27.7	209.58
Kakadu	KDU	-12.69	132.47	-21.4	206.3
Kanoya	KNY	31.42	130.88	22.24	201.54
Kourou	KOU	5.21	307.27	14.33	20.39
Kototabang	KTB	-0.2	100.32	-9.87	172.75
Learmonth	LRM	-22.2	114.1	-31.74	187.24
Lanzhou	LZH	36.1	103.84	26.19	176.73
Mbour	MBO	14.38	343.03	19.63	58.06
Middlemarch	MDM	-45.6	170.09	-49.16	252.42
Moshiri	MSR/MOS	44.37	142.27	35.95	210.38
Pedeli	PEG	38.1	23.9	36.2	103.71
Phuthuy	PHU	21.02	105.95	11.16	178.56
Pamatai	PPT	-17.57	210.42	-15.04	285.72
Shillong	SHL	25.57	91.88	16.01	165.38
Silchar	SIL	24.68	92.75	15.09	166.16
San Juan	SJG	18.12	293.85	27.69	6.87
Tamanrasset	TAM	22.79	5.53	24.32	82.25
Te Wharau	TEW	-41.18	175.83	-43.91	256.91
Tucson	TUC	32.17	249.27	39.43	317.25

Table 2
List of Pi2 Events

No	Event	UT	Swarm satellite	Geomagnetic latitude	MLT
1	4 April 2014	17:15–17:25	A	NA	NA
			B	17.9° S to 55.4° S	14.7
			C	13.9° S to 24.1° N	2.8
2	6 April 2014	22:43–22:53	A	28.8° S to 9.2° N	2.5
			B	60.0° N to 22.7° N	14.2
			C	8.7° N to 46.5° N	3.0
3	12 April 2014	00:54–01:01	A	24.4° S to 1.7° S	2
			B	12.6° S to 35.1° S	14.8
			C	19.5° S to 3.2° N	2.1
4	25 April 2014	14:38–14:43	A	50.0° S to 31.1° S	1.0
			B	67.1° N to 48.6° N	13.6
			C	49.0° S to 30.4° S	1.1
5	2 August 2014	14:07–14:16	A	32.3° S to 1.7° N	15.5
			B	50.3° N to 16.8° N	3.8
			C	32.1° S to 1.9° N	15.6
6	8 August 2014	05:30–05:37	A	46.2° N to 19.6° S	3.5
			B	34.2° S to 8.0° S	16.2
			C	45.6° N to 19.0° N	3.6
7	13 August 2014	06:48–06:56	A	54.5° S to 24.0° S	14.9
			B	19.5° S to 49.6° S	3.5
			C	54.1° S to 23.5° S	15.0
8	14 August 2014	17:57–18:08	A	52.2° N to 10.3° N	2.5
			B	65.8° S to 25.0° S	15.0
			C	51.9° N to 10.0° N	2.6
9	1 September 2014	19:39:30–19:45:30	A	31.6° N to 8.7° N	1.4
			B	32.3° S to 9.6° S	14.2
			C	31.2° N to 8.3° N	1.5
10	3 September 2014	02:32–02:38	A	33.7° N to 56.4° N	12.8
			B	41.1° N to 18.8° N	2.2
			C	34.1° N to 56.8° N	12.9
11	20 September 2014	14:29–14:42	A	22.5° N to 27.2° S	23.6
			B	60.2° S to 11.8° S	11.8
			C	22.4° N to 27.3° S	23.6
12	25 September 2014	06:17–06:27	A	62.6° S to 24.9° S	10.9
			B	19.6° N to 18.2° S	0.3
			C	62.5° S to 24.8° S	11.0
13	1 October 2014	15:36–15:45	A	58.2° S to 23.9° S	10.6
			B	35.4° N to 1.2° N	23.6
			C	57.9° S to 23.6° S	10.7
14	24 October 2014	15:16:30–15:23:30	A	40.7° N to 14.0° N	20.9
			B	39.7° N to 66.2° N	9.8
			C	40.2° N to 13.4° N	21.0
15	26 October 2014	05:42:30–05:47:30	A	29.9° S to 11.0° S	8.4
			B	48.7° N to 30.0° N	21.3
			C	29.7° S to 10.8° S	8.6

Note. MLT = magnetic local time.

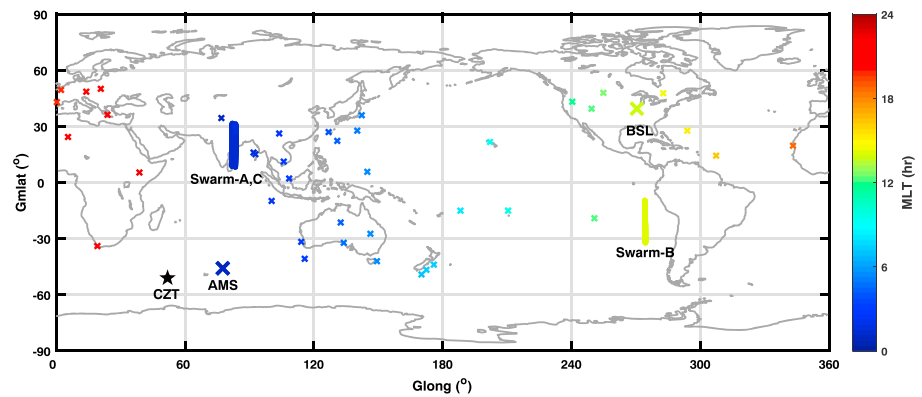


Figure 1. Map depicting the relative location of the Swarm satellites (thick line) and 43 ground stations (shown by small “x”) during the Pi2 event on 1 September 2014. The magnetic local time (MLT) at each location is indicated by the color bar. The underneath and midnight ground stations considered for the event are indicated by the symbols, large “x” and black star, respectively.

coordinates to get the magnetic field variations in compressional (Bcomp—along the magnetic field and positive north), poloidal (Bpol—perpendicular to the magnetic field and positive radially down), and toroidal (Btor—perpendicular to the magnetic field and positive azimuthally east) components. The residual fields in different magnetic field components at satellite obtained using CHAOS 5 are also compared with that obtained using latest CHAOS 6 model (Finlay et al., 2016) and are found to be identical.

2.3. Pi2 Event Identification

Pi2 events are primarily identified using ISEE (Institute for Space-Earth Environmental Research) fluxgate magnetometer data from the Moshiri observatory (MSR/MOS; 44.37° N, 142.27° E) together with the Wp (Wave and planetary) and AL (Auroral Lower) indices during the period January–December 2014. Wp is a substorm index developed by Nose et. al. (2009, 2012), which measures Pi2 spectral power at low latitudes. An increase in Wp, together with a depression in AL indicates the occurrence of substorm associated Pi2 oscillations at low latitudes. During the intervals, when Wp (AL) index shows sudden increase (decrease), the magnetic field variations in *H* component from MSR ground station band-pass filtered in the Pi2 frequency range (6.6–25 mHz) is visually checked to confirm Pi2 oscillations. For the events identified when the MSR station was located outside the night (20:00–04:00) LT (i.e., at day, dawn, or dusk LT), the *H* oscillations at MSR are compared with that of a low-latitude station located near midnight. High values of coherence (coherence > 0.6) in the *H* oscillations between two ground stations, with larger amplitudes in the nightside have been used to ensure that the selected event is a Pi2 event. Following this procedure, we identified 525 Pi2 events at MSR, with 280 identified when MSR was located at night and 245 during day and terminator LT.

Once Pi2s are identified at ground, they are further compared with Swarm observations. Criteria imposed for the selection of Pi2 event at the Swarm satellite are as follows. (1) Simultaneous observations at Swarm from day (8–16 hr) and night (20–4 hr) LT sectors. (2) Coherent oscillations (coherence > 0.6) in the compressional component at the satellite (in day and night) and *H* component at MSR. (3) Swarm satellites located within $\pm 65^\circ$ geomagnetic latitudes during the Pi2 event. (4) In the dayside, the satellites crossing dip equator are not considered in order to avoid the interference of equatorial electrojet signatures.

With these four criteria, we obtained 15 Pi2 events, for which Swarm satellites were simultaneously located in day and night sectors, and the compressional component at day and night satellite showed coherent oscillations with MSR *H*. Table 2 gives the list of 15 Pi2 events considered in this study.

3. Case Study of Pi2 Pulsations

This section presents two cases of Pi2 events in detail. The first event illustrates the analysis procedure that is applied to all 15 events. The second event depicts the global view of Pi2 oscillations simultaneously observed from Swarm satellites and ground stations. It is to be noted that in the present analysis, the band-pass filter in the frequency range 6.6–25 mHz is applied only for the visual inspection of the satellite and ground observations. However, for the spectral analysis, that is, for the computation of power spectral density, coherence, and cross phase, a broader pass band of 3–50 mHz is used to avoid any modulation of the fre-

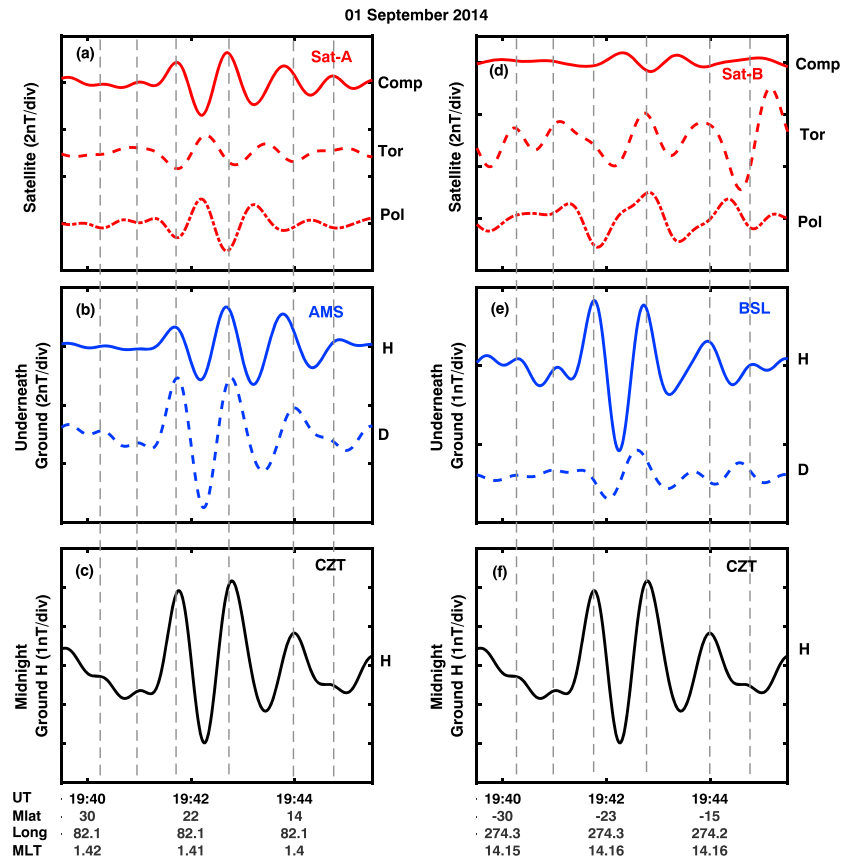


Figure 2. Pi2 event on 1 September 2014. Comparison of Pi2 oscillations observed by Swarm A (a) and Swarm B (d) satellites in the compressional (solid red curve), toroidal (dashed red curve), and poloidal (dashed dotted red curve) components with H (solid blue curve) and D (dashed blue curve) components from underneath ground stations, AMS (b) and BSL (e) along with H component (solid black curve) from midnight ground station CZT (c, f). Swarm A and the AMS were located in the nightside, and Swarm B and BSL were located in the dayside. CZT is the midnight ground station. Ground stations CZT and AMS are located in the SH, and BSL is located in the NH. The UT of the event, magnetic latitude, geographic longitude, and magnetic local time (MLT) of the Swarm satellites are mentioned at the bottom.

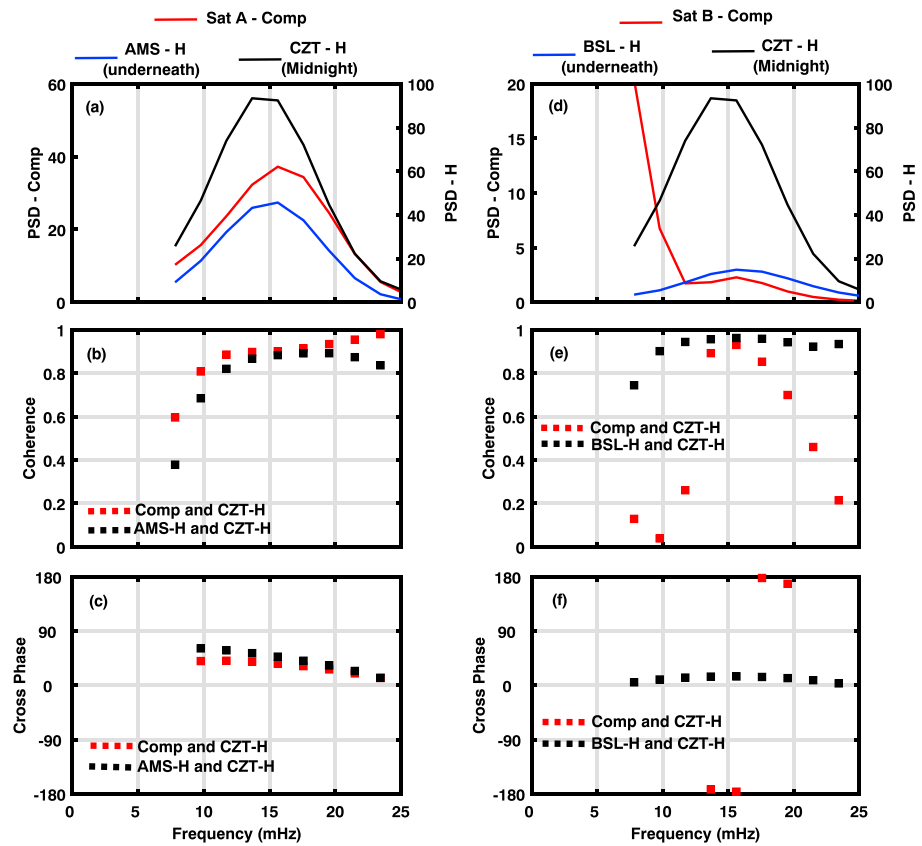
quencies of interest. The band-pass filter used in this analysis is the frequency domain filtering. We applied a boxcar/rectangular window to the signal in frequency domain, which is then converted to the time domain by applying an inverse Fourier transform.

3.1. Pi2 Event on 1 September 2014

3.1.1. Pi2 Oscillations in All Three Components at Satellite and Comparison With Ground H and D

The first event presented here occurred on 1 September 2014 with Pi2 onset shortly after 19:40 UT. During the event Swarm A/C and Swarm B satellites were located in the night and day LT sectors, respectively. Figure 1 presents the location of the Swarm satellites (thick lines) during the event along with all ground stations listed in Table 1 (shown by symbol small “x”). The ground stations located closest to the satellite longitudes (underneath stations) and that located near midnight meridian are highlighted in the map by the symbols large “x” and black star, respectively. The color bar indicates the magnetic local time (MLT) at each location during the event.

The filtered (6.6–25 mHz) time series depicting the Pi2 signatures in different magnetic field components observed at satellite and ground are presented in Figure 2. As Swarms A and C were located very close to each other, the magnetic field signatures at both are nearly identical. Hence, only observation from Swarm A in the nightside and Swarm B in the dayside are presented here. Top panels (a) and (d) show the magnetic field oscillations at satellites Swarm A (hereafter mentioned as Sat A) and Swarm B (Sat B), respectively in the compressional (solid red curve), toroidal (dashed red curve), and poloidal (dotted dashed red curve)



01 September 2014

Figure 3. Pi2 event on 1 September 2014. Spectral characteristics of the compressional component at Sat A (a–c) and Sat B (d–f) along with H component at underneath and midnight ground stations. (top rows) The power spectral density (PSD) of the compressional component at satellites (red curves) and H component at underneath (blue curves) and midnight (black curves) ground stations. (middle rows) Coherence and (bottom rows) cross phase between satellite compressional and midnight ground H (red squares); the values between underneath and midnight ground H are shown by black squares.

components. The middle panels (b) and (e) depicts the oscillations in the H (solid blue curve) and D (dashed blue curves) components from ground stations underneath each satellite. In addition to the underneath ground, Pi2 oscillations at Swarm satellites in the day and night LT are also compared with the H oscillations at a ground station located near midnight meridian (black solid curve) and is shown in the bottom panels (c) and (f), which is hereafter referred as midnight station. The underneath ground stations for Sat A and Sat B are AMS and BSL, respectively, and the midnight station is CZT. During the event, Sat A and AMS were located in the postmidnight sector, with mean MLT 1 hr and Sat B and ground BSL were in the afternoon hours with mean MLT 14 hr. UT of the event and the location of the satellites, that is, magnetic latitude (Mlat), geographic longitude (Long), and MLT are shown at the bottom of each panel.

Pi2 signatures in the compressional, toroidal, and poloidal components (red curve) at Sat A showed matching oscillations (coherence > 0.6) with H and D components at underneath ground station (AMS; blue curves) and H component at midnight station (CZT; black curve). This clearly demonstrates the presence of identical Pi2 oscillations in the compressional, toroidal, and poloidal components in the topside ionosphere and H and D components at ground during night hours. The compressional component at Sat A showed in-phase, and poloidal component showed antiphase oscillations with H component at both underneath and midnight ground stations. It is to be noted that, in addition to the compressional and poloidal components, coherent Pi2 oscillations are also present in the toroidal component at Sat A. The toroidal oscillation at satellite also has strikingly identical signatures with AMS D , indicating the presence of identical Pi2 oscillations in the azimuthal components at topside ionosphere and ground. The toroidal component oscillates

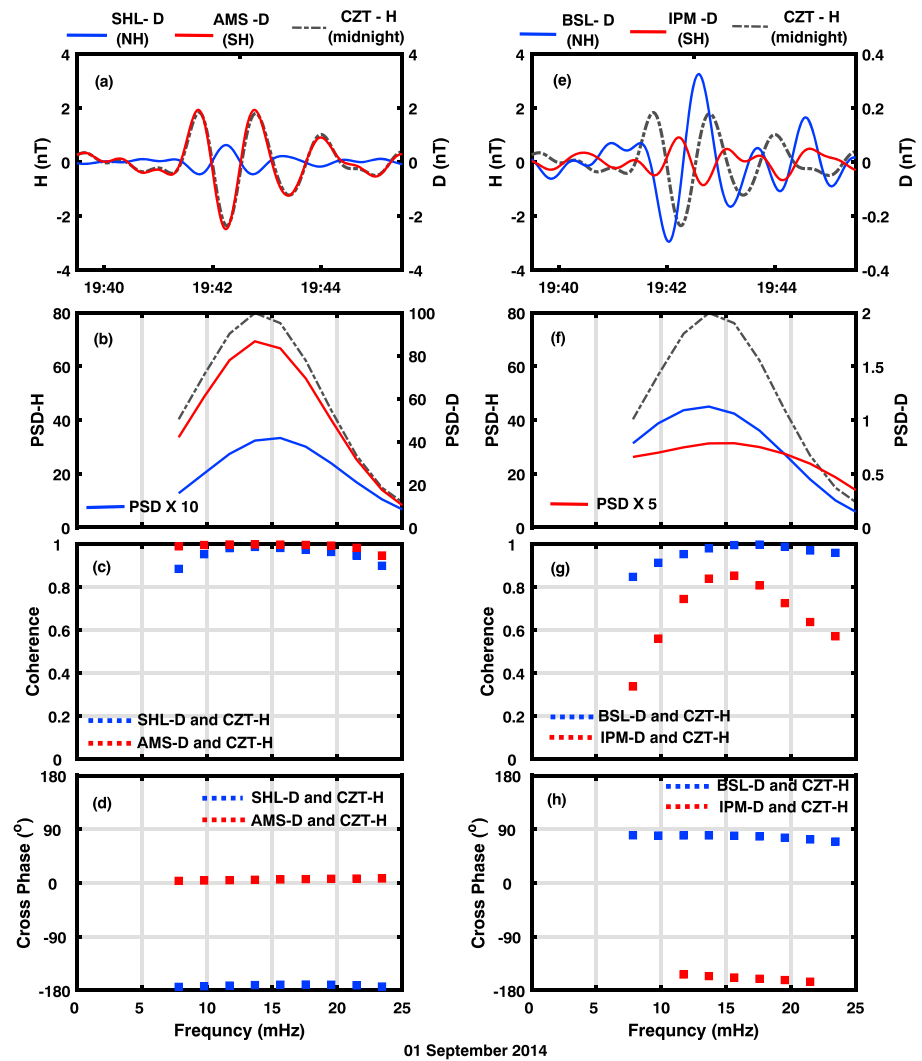


Figure 4. Pi2 event on 1 September 2014. Spectral characteristics of Pi2 oscillations in the ground D component at day and night LTs in different hemispheres. SHL and AMS represent Northern (NH) and Southern (SH) Hemispheric stations, respectively, in the night sector (a–d). Ground stations BSL (NH) and IPM (SH) are used in the day sector (e–h). (first row) Time series and (second row) power spectral density (PSD) of the D components in the NH (blue curve) and SH (red curve) together with midnight ground H (dashed gray curve). (third row) The coherence and (fourth row) the cross phase of NH- D (SH- D) with midnight H are shown by blue squares (red squares).

antiphase with AMS D and midnight H . It is to be noted that during the event, Sat A was purely in the NH. However, AMS ground station is located in the SH.

In the dayside, compressional oscillation at Sat B show matching but antiphase signatures in comparison with H at underneath ground station (BSL). Oscillations in the dayside satellite and ground are also matching with midnight ground H . This clearly demonstrates the simultaneous occurrence of Pi2 pulsations in day and night hours both above and below the ionosphere. It is interesting to note that the phase relation observed between satellite compressional and ground H is out of phase during day and in phase during night LTs.

During daytime, the Pi2 oscillations in the poloidal component is found to have less match with ground H (coherence < 0.6). The oscillation in the toroidal component is also found to be different from midnight H and BSL D resulting in coherence less than 0.6.

3.1.2. Spectral Analysis of Satellite Compressional and Ground H

Figure 3 depicts the spectral characteristics of the Pi2 pulsations in the satellite compressional and ground H components for the event shown in Figure 2. Top panels show the power spectral density (PSD) of Pi2

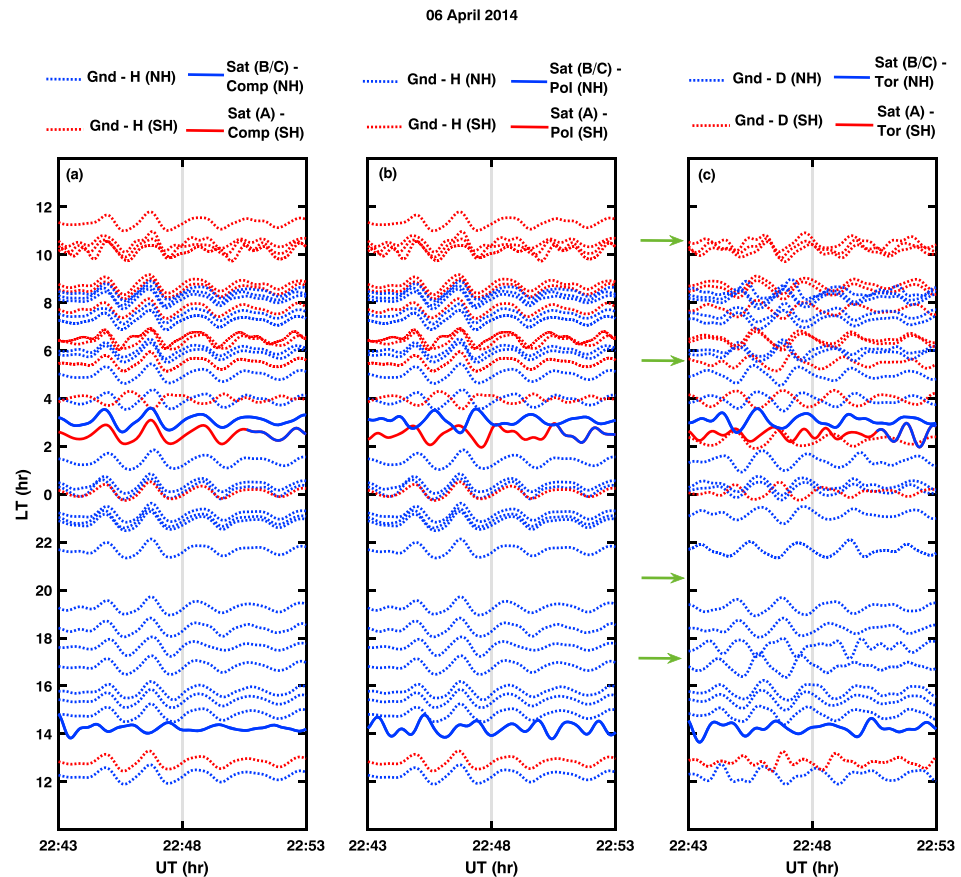


Figure 5. An example of the Pi2 oscillations observed on 6 April 2014 in the compressional (left), poloidal (middle), and toroidal (right) components at Swarm satellites (solid line) and *H*, *H*, and *D* components (dotted line), respectively, at different ground stations distributed in local time (LT). Blue and red colors indicate Northern Hemisphere (NH) and Southern Hemisphere (SH) locations.

at satellites (red solid curve) in the day and night LT sectors together with midnight (black solid curve) and underneath (blue curve) ground stations in the same colors as Figure 2. During nighttime, Sat A and the ground stations (AMS and CZT) showed identical frequency peak at ~ 15 mHz, with maximum Pi2 power at midnight ground station (Figure 3a). Presence of identical frequency results in a good coherence (Figure 3b) between satellite compressional and midnight *H* (red squares) and also that between *H* at two ground stations (black squares). Cross phase (Figure 3c) between satellite and ground (red squares) and that between ground and ground (black squares) are found to be $\sim 45^\circ$ indicating near in-phase oscillations at satellites and ground stations placed at night. The dayside observations from Sat B and BSL also showed frequency peaks identical to midnight *H*. However, an additional frequency contribution unique to Sat B is evident in the lower frequency band of Pi2 below 10 mHz. At Pi2 frequency, coherence between Sat B compressional component and midnight ground *H* is found to be ~ 0.9 and that between *H* components at day and night ground is >0.9 . Cross-phase angles clearly indicate nearly in-phase ($\sim 20^\circ$) oscillations in the *H* component at day and night ground stations and out-of-phase ($\pm 180^\circ$) oscillations between Sat B and midnight *H*.

3.1.3. Spectral Analysis of Ground *D* Variations

In order to understand Pi2 oscillations in the *D* component, ground stations from NH and SH, located underneath Sat A in the nighttime (mean LT of ground stations: 1.3 hr) and Sat B in the daytime (mean LT of ground stations: 13.0 hr) are considered. Figure 4 presents the time series and the spectral characteristics of ground *D* oscillations in comparison with midnight *H* variations. Left panels show the observations from ground stations in the nightside, and right panels show that in the dayside. It is to be noted that in the first and second rows, the *H* values are marked in the left-hand scale and the *D* values in the right-hand scale.

D components in the NH (blue solid curve) and SH (red solid curve) showed matching oscillations with midnight H (dashed gray curve) in both night (Figure 4a) and day (Figure 4e) hours. PSD depicts the presence of identical Pi2 frequency peaks at ~ 15 mHz in H and D components resulting in good coherence (coherence > 0.6). Note that the PSD at SHL station is multiplied by 10 and that at IPM station is multiplied by a factor of 5. In the nightside, the PSD of D variations at SHL (located at NH) is found to be much smaller than that of AMS (located at SH). Similarly in the dayside, the PSD of IPM in the SH is found to be smaller than BSL in the NH. It is to be noted that SHL and IPM are located at relatively lower latitudes, compared to AMS and BSL (Table 1). This may indicate that the Pi2 oscillations in the D component has smaller amplitude at low latitude in comparison to the relatively higher latitude stations.

In the nightside (postmidnight hours), the the cross phase (Figure 4d) depicts nearly out of phase oscillations between D components in the NH (SHL) and SH (AMS) stations, with SHL- D oscillating antiphase (blue squares) and AMS- D oscillating in phase (red squares) with midnight (CZT) H . Dayside observations (afternoon hours) also showed nearly antiphase oscillations in D across hemispheres but in opposite sense with nighttime observations (Figure 4h). That is, in the afternoon hours, the D variations in the SH (IPM- D) showed nearly out-of-phase oscillations and that in the NH (BSL- D) showed a phase shifted ($\sim 70^\circ$) oscillation with midnight (CZT) H . This implies that apart from phase reversal between hemispheres, Pi2 signatures in D component follow different phase patterns across LT.

3.2. Pi2 Event on 6 April 2014

3.2.1. LT and Hemispheric Dependence of Pi2s at Satellite and Ground

Figure 5 presents case study of the second event occurred on 6 April 2014 with Pi2 onset at 22:44 UT. Figure shows the time profiles of Pi2 oscillations in different MLT sectors, recorded from all the available satellite and ground platforms. Ground observations are obtained from the observatories listed in Table 1, located within $\pm 51^\circ$ geomagnetic latitudes. In Figure 5, satellite and ground observations are indicated by solid and dotted lines, respectively. Blue and red colors are used to denote the Northern and Southern Hemispheric locations. The left panel (Figure 5a) shows the satellite compressional and ground H variations. Satellite poloidal along with ground H components are displayed in the middle panel (Figure 5b), and the right panel (Figure 5c) shows the satellite toroidal and ground D variations. The Pi2 oscillations at each location (ground station and satellite) are normalized by the maximum value of the amplitude at that particular location. Pi2 variations in H and D components, which have coherence > 0.6 with midnight ground H are only displayed in the figure. During the event, Sat A and Sat C were located in the postmidnight hours (mean MLT for Sat A and Sat C are 2.5 and 3.1 hr, respectively), with Sat A moving from $\sim 27^\circ$ S to 3.5° N and Sat C purely in the NH moving from 10.6° N to 41° N. At the same time, Sat B was located in the dayside (mean MLT: 14.3 hr) moving from 58° N to 28° N. In the nightside, Sat A and Sat C were located in the opposite hemispheres, at least during the main part of the Pi2 impulse (22:44 to 22:51 UT). This makes the event interesting as it provides an opportunity to understand how different components of Pi2 oscillations behave in different hemispheres, at the topside ionosphere.

It can be noted from Figure 5a that ground H component show similar and nearly in-phase oscillations, irrespective of the LT (day, night, dawn, and dusk times) and latitude of the ground station. However, there is an exception near 4 LT, where H component at an SH ground station show antiphase variation. Satellites A and C located in the nightside but at opposite hemispheres also show similar and in-phase oscillations with ground H . However, Sat B located in the daytime (mean MLT: 14.3 hr) show similar but antiphase oscillation with ground H . This indicates that unlike ground H , compressional oscillations in the topside ionosphere undergo a phase reversal between day and night LT.

Panel (b) shows the comparison of poloidal component with ground H . It can be noticed that nighttime satellite passes show similar and coherent oscillations in the poloidal component with those at ground H . It is interesting to note that poloidal component show opposite signatures in the NH (Sat C) and SH (Sat A), during nighttime. The daytime observations (Sat B) of poloidal component also show nearly matching but phase shifted Pi2 signatures with ground H .

Pi2 signatures are found to be present in the toroidal and D components (Figure 5c). Unlike H , the oscillations in the D component on ground are not in phase all over the globe. They are observed to have different phase dependence at different LT and hemispheres. For a given LT, the D observations from two different hemispheres are found have opposite phase. Apart from hemispheric difference, phase reversal in D is also evident at four LT locations and are marked in the figure with four green arrows. Phase reversal is observed

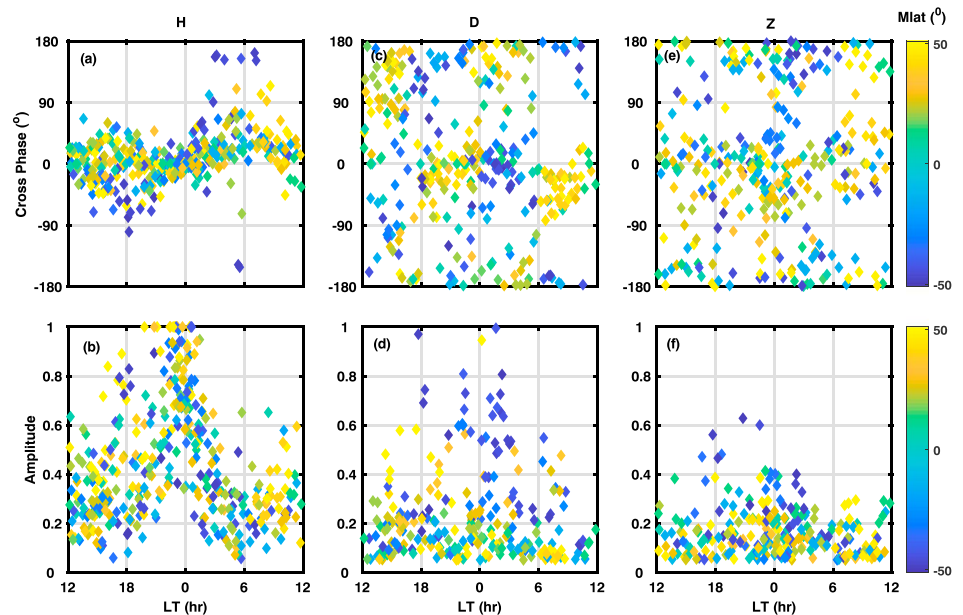


Figure 6. Local time (LT) dependence of the cross phase (top row) and amplitude (bottom row) of Pi2 oscillations at ground with coherence > 0.6 relative to midnight ground H , in H (a, b), D (c, d), and Z (e, f) magnetic field components.

in the dawn sector between 5 and 6 LT and in the dusk sector between 17 and 18 LT. In addition, the phase reversal took place at prenoon hours between 11 and 12 LT and in the night sector between 19 and 22 hr. Due to the lack of observations at LT between 19 and 22 hr, only a broad LT range could be specified for nighttime phase reversal. In general, the toroidal components at Sat A and Sat C show oscillations similar to ground D at night with opposite phase between NH and SH. However, toward the end of the Pi2 wave cycle (UT: 22:47:30–22:51:30), when Sat A (solid red line) was at very low latitudes, and crossing equator, the Pi2 oscillations in the toroidal component is found to be modified. During daytime, the toroidal component is found to have matching Pi2 oscillations with ground D . The phase of the toroidal oscillations at Sat B, located in the NH and in the postnoon hours is found to be nearly opposite with ground D oscillations in the NH station at nearby LT.

4. Statistical Results

In this section, we present the results obtained from all 15 events considered in the present study. Here we have determined the amplitude and cross phase of the Pi2 oscillations in all three components (H , D , and Z for ground observations and compressional, poloidal, and toroidal for satellite observations), which showed coherent oscillations with corresponding midnight ground H (coherence > 0.6). The statistics of the characteristics of Pi2s are depicted in Figures 6–8, where the magnetic latitudes of the observation points are indicated by color bar. For the sake of comparison, the amplitude of the Pi2 oscillations in all the three components at both satellite and ground are normalized by the maximum H amplitude for each event.

4.1. Ground Observations (H , D , and Z Components)

Figure 6 presents the LT variation of the cross phase (top row) and amplitude (bottom row) of Pi2 oscillations in H (left panels), D (middle panels), and Z (right panels) components observed on the ground stations. Note that the cross phases are computed with respect to midnight H variations. One can observe that in general, the H oscillations observed at different ground stations are nearly in phase ($\leq 90^\circ$) with midnight H (Figure 6a). However, larger phase differences are evident in the postmidnight to dawn hours ($\sim 180^\circ$), particularly for the stations at higher latitudes. Beyond dawn (6 hr) LT, the cross phase appears to decrease steadily and becomes nearly 0° around noon. Although not dominant, a similar phase change is also apparent in the dusk sector with cross phase changing between 0° and -100° . Thus, our observations suggest that, particularly at latitudes $> \pm 40^\circ$, the H component tends to have a phase reversal at LT between postmidnight (premidnight) to dawn (dusk) terminator hours.

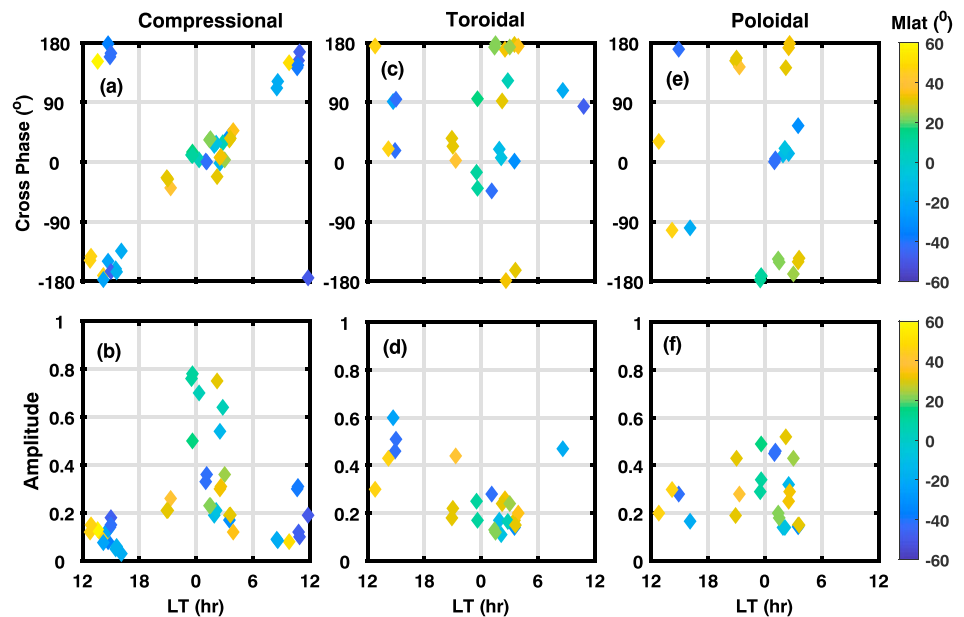


Figure 7. Local time (LT) dependence of the cross-phase (top row) and amplitude (bottom row) of Pi2 oscillations at satellite relative to midnight ground H in the compressional (a, b), toroidal (c, d), and poloidal (e, f) magnetic field components.

The amplitude of H oscillations (Figure 6b) is found to be maximum in the premidnight hours between 20 and 24 LT, and has minima near dawn and dusk hours. In the postmidnight to dawn hours, the Pi2 amplitude is found to decrease steadily with less scatter and attains minimum near 6 LT. However, a large scatter in the amplitude is evident in the dusk sector. These observations show that H component undergo significant decrease in the amplitude and increase in the phase near terminators. The difference in the Pi2 characteristics observed at dawn and dusk sectors may indicate the asymmetry in the H oscillations at these LTs.

Characteristics of Pi2 in the D component are depicted in the middle panel (Figures 6c and 6d). Note that the color bar indicates the location of the ground stations in NH and SH. The cross phase of D with midnight H is observed to be structured in both LT and latitude. It can be observed from Figure 6c, that in the premidnight hours between 18 and 0 LT, the cross phase is $\sim 0^\circ$ in the NH and $\sim 180^\circ$ in the SH. Beyond midnight between 0 and 6 LT, the phase of D oscillations appears to reverse, with NH showing out-of-phase and SH showing in-phase oscillations with H . Apart from the nightside LTs, a similar but opposite phase reversal is also clearly observed in the dayside LTs (6–18 LT) across the noon meridian, with D component showing in-phase (out-of-phase) oscillation in the NH (SH) during prenoon hours at 6–12 LT. During the postnoon hours at 12–18 LT, the oscillations are out of phase in the NH; however, no clear phase variations are evident in the SH. Thus, it can be inferred from the Figure 6c that phase of D oscillations associated with Pi2 has a strong dependence on LT, with clear phase reversals near noon, dawn, midnight, and dusk meridians. The phase of D is also found to be opposite across the hemispheres at all LTs, indicating that the source of Pi2 associated D variations is symmetric about the equator.

The normalized amplitude of the D oscillations (with respect to the midnight H) greater than 0.01 are displayed in Figure 6d. The amplitude of D component in general appeared to have larger values at night (18–6 LT) compared to day, with isolated large variations present around the dusk terminator at ~ 18 LT and in the postmidnight hour at ~ 3 LT. In the night hours between 18 and 3 LT, the D amplitude is found to have more scatter from 0.1 to 1, and therefore, a clear dependence on LT could not be identified. However, it is evident from the observations that D component has larger amplitude at middle-low latitudes compared to equator to very low latitudes.

In order to get a 3-D picture of Pi2 oscillations, in addition to H and D , we also investigated the variations in the Z component. In our analysis, the Pi2 associated Z oscillations are often observed to have matching signatures with H at midnight ground, resulting in good coherence. The cross phase and amplitude of these

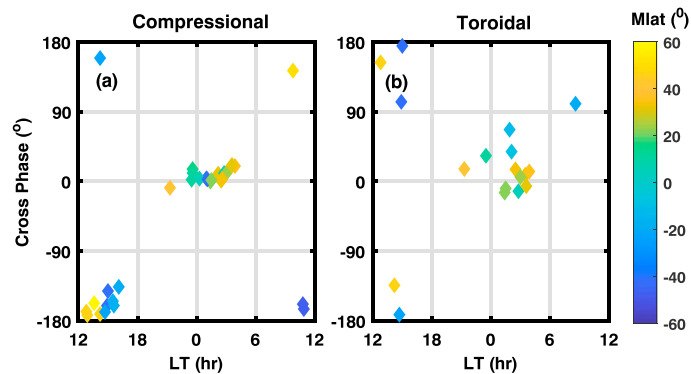


Figure 8. Local time (LT) dependence of the cross phase of the (a) compressional and (b) toroidal magnetic field components relative to underneath ground H and D , respectively.

coherent oscillations observed in the Z component are presented in Figures 6e and 6f. Although coherent signatures were identified in the Z component, its cross phase with midnight H seems to have no systematic pattern in LT. In general, the phase of Z oscillations appeared to be clustered around 0° and $\pm 180^\circ$ at all LTs. During night hours, between 18 and 6 LT through midnight, a vague phase relation between Z and H components are observed with majority of NH stations showing in-phase and SH showing out-of-phase oscillations. During day hours, the observations were mostly from NH stations, which showed both in-phase and out-of-phase oscillations between Z and H , and hence, no systematic dependence. In Figure 6f, there is an enhancement of Z amplitude in the premidnight hours.

4.2. Satellite Observations (Compressional, Poloidal, and Toroidal Components)

The LT variation of the cross phase and amplitude of Pi2 in the compressional, poloidal, and toroidal components observed by the Swarm satellites at the topside of the ionosphere during all the 15 Pi2 events are presented in Figure 7 in the same format as Figure 6. Figure 7a shows the cross phase between satellite compressional and midnight ground H . The satellite compressional and midnight ground H are observed to be oscillating in phase at night and nearly out of phase at day, irrespective of the latitude. This implies, the compressional oscillations in the topside ionosphere have $\sim 180^\circ$ phase difference between day and night LT sectors. The amplitude of the compressional oscillations is normalized with maximum H amplitude at ground and is depicted in Figure 7b. In general, the amplitude of compressional component is found to be larger at night compared to day. Also, the observations in the postmidnight hours showed a clear decreasing trend in the compressional amplitude from midnight toward dawn hours.

For more than 80% of the Pi2 events, the toroidal (azimuthal) and poloidal (radial) components observed in the nightside showed coherent oscillations with midnight ground H , but the same was not found to be true during day. It can be noted that the cross phase of satellite toroidal (azimuthal) oscillations in Figure 7c is analogous to ground D . At night, the toroidal oscillations at satellite observed mostly in the postmidnight hours showed nearly in-phase oscillations in the SH and nearly antiphase oscillations in the NH. It is interesting to note that the cross phase of toroidal oscillations in the premidnight hours is opposite to that of postmidnight sector, with the toroidal oscillations in the NH showing nearly in-phase oscillation with midnight H . These observations in the toroidal component are found to be similar to that of D in the premidnight and postmidnight hours depicting identical azimuthal variations at satellite and ground during nighttime. During day, unlike ground, the toroidal oscillations at satellite did not show any systematic phase relation with the midnight ground H . The toroidal oscillations (Figure 7d) in general appeared to have smaller amplitudes at night compared to day.

As depicted in Figure 7e, the poloidal component at night (both premidnight and postmidnight sectors) is observed to oscillate out of phase in the NH and in phase in the SH with midnight ground H . This indicates a phase reversal in the poloidal oscillations across equator at night, similar to the D and toroidal oscillations at ground and satellite, respectively. However, it is important to note that unlike D and toroidal, the poloidal oscillations did not show phase reversal across midnight meridian. During daytime, only a few events showed coherent oscillations in the poloidal component.

These observations in the poloidal (radial) component at satellite are found to be different from that at ground Z component shown in Figure 6e. During night, when radial (poloidal) magnetic field at satellite showed clear in-phase and out-of-phase oscillations at SH and NH, respectively, ground showed a vague but opposite phase relation. The amplitude of poloidal oscillations (Figure 7f) at satellite are in general observed to be comparable with the compressional ones during night hours.

4.2.1. Cross Phases Between Satellite and Underneath Ground Station

The Pi2 oscillations in the compressional and toroidal components at satellite are also compared with H and D components, respectively, from underneath ground stations. Figure 8 depicts the LT variation of the cross phase between the analogous components, that is, compressional and H (Figure 8a) and toroidal and D (Figure 8b) at Swarms A–C satellites and the corresponding underneath station. As Swarms A and C were mostly orbiting in the nearby latitude and longitude, the underneath ground station used for Swarm A/C are same except for one event when both were in opposite hemispheres. As D component is found to have clear hemispheric dependence, the underneath ground station considered here is selected from the same hemisphere as that of satellite and that located within $\pm 20^\circ$ longitude of the satellite.

Figure 8a demonstrates nearly in-phase oscillations at night and antiphase oscillations near noon between satellite compressional and underneath ground H . It is interesting to note that the toroidal component also has similar phase relation with D component from underneath ground stations, with nearly in-phase oscillations at night and nearly antiphase oscillations during day. It is therefore clearly evident from Figure 8 that the satellite and ground witnessed identical oscillations at nighttime and identical but opposite oscillations during day.

5. Discussion

The present study carries out for the first time, the Pi2 observations from a dense network of low-middle latitude ground stations covering all LT sectors together with multisatellite observations from the topside ionosphere. One of the distinct advantage of employing conjugate observations from the satellites in the topside ionosphere and ground is that we can identify the role of the ionosphere in modifying the Pi2 waves. If Pi2 is caused by an impulsive hydromagnetic fast-mode wave, it will be manifested mostly in the compressional and poloidal components, which gets mapped to the H component at ground (Takahashi et al., 1995). This may be true for an idealistic condition of azimuthal wave number, $m = 0$. For $m > 0$, the compressional oscillations can get coupled with the toroidal (or shear Alfvén) mode (Kivelson & Southwood, 1986; Southwood, 1974), when the eigenfrequency of cavity matches with the field-line eigenfrequency, thereby leading to the field line resonance. However, field line resonances, which are mostly toroidal resonances will be observed in the azimuthal component above the ionosphere. According to Kivelson and Southwood (1988), the ionosphere will introduce a 90° rotation on these waves and will therefore be manifested in the H component at ground. Our observations of Pi2s from space and ground in all the three magnetic field components provide an important perception about the wave type responsible for the generation of low-middle latitude Pi2 oscillations. The following subsections discuss the present observations along with the responsible mechanisms in detail, for different LT sectors separately.

5.1. Nighttime Pi2

The simultaneous observations in the compressional/ H , toroidal/ D , and poloidal/ Z magnetic field components at satellite and ground enabled us to get a three-dimensional view of Pi2 oscillations at middle and low latitudes. Our observations of nighttime Pi2 signatures are found to follow the magnetic field pattern of the oscillating SCW FAC. The observations of our nighttime Pi2s will be compared and discussed in view of oscillating SCW model.

5.1.1. Brief Review of Nighttime Pi2 Models

This section briefly introduces three different Pi2 models, that is, (a) plasmaspheric cavity resonance, (b) forced oscillation by external driver, and (c) oscillating SCW.

5.1.1.1. Plasmaspheric Cavity Resonance

The plasmaspheric cavity resonance is a dominant model that explains the nighttime low-latitude Pi2 pulsations (Saito & Matsushita, 1968). Many observational results from ground (Lin et al., 1991; Nosé et al., 2006; Sutcliffe & Yumoto, 1991; Yeoman & Orr, 1989; Yumoto, 1990) and space platforms (Keiling et al., 2014; Nosé et al., 2003; Sutcliffe & Lühr, 2003; Takahashi et al., 1995, 1999; Teramoto et al., 2011) together with numerical calculations (Allan et al., 1986, 1996; Fujita et al., 2002; Lee, 1996) have proposed cavity oscillations excited by the compressional fast-mode waves inside the plasmasphere as a possible source mechanism

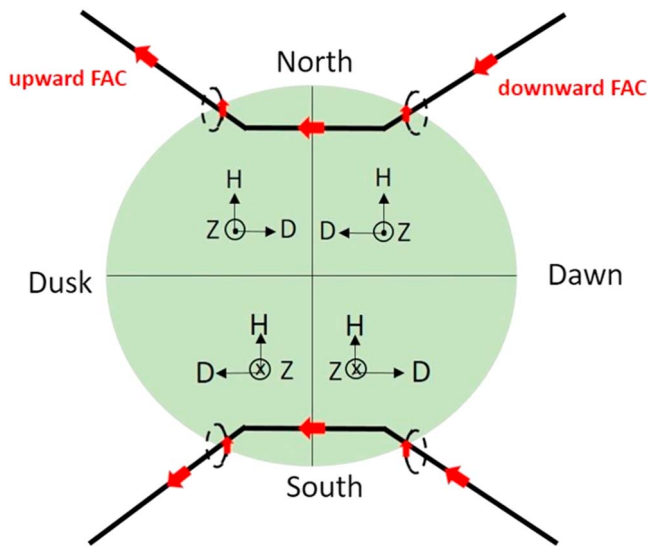


Figure 9. Schematic representation of the nightside view of field-aligned current (FAC) and ionospheric current geometry of the one phase of oscillating substorm current wedge and the predicted directions of the associated magnetic field perturbations in H (horizontal), D (azimuthal), and Z (radial) directions in geomagnetic coordinates.

responsible for nighttime low-latitude Pi2s. Space-borne observations by Takahashi et al. (1992), Takahashi et al. (1995), and Teramoto et al. (2011) using Active Magnetospheric Particle Tracer Explorers/Charge Composition Explorer and by Takahashi et al. (1999, 2001) using Combined Release and Radiation Effects Satellites in the equatorial magnetosphere reveal that Pi2 oscillations are dominated by the compressional and poloidal components in the equatorial plane and are confined to the radial distances within the plasmasphere. These results support the idea that Pi2 oscillations are caused by plasmaspheric cavity resonance. However, the observations by Osaki et al. (1998) using Akebono satellite in the off-equatorial latitudes reveals a completely different picture of nighttime Pi2s. Their observations shows that in the inner magnetosphere, Pi2 oscillations are polarized to transverse components beyond $\pm 20^\circ$ Mlat. Different observations from magnetospheric satellites in the equatorial and off-equatorial plane can provide significant insights on the latitudinal extent of plasmaspheric cavity oscillations. As the compressional source region is localized to equatorial plane in the plasma sheet, the cavity resonance excited by these compressional fast-mode wave may be confined to the equatorial latitudes.

5.1.1.2. Forced Oscillation by External Driver

Pi2 oscillations are also believed to be a result of the forced oscillation by an oscillatory source external to the magnetosphere. Itonaga and Yoshikawa (1996) suggested that the transient response of the inner magnetosphere/plasmasphere to the Earthward propagating compressional

oscillations (confined to midnight LT and to equatorial latitude) excited by a large-scale oscillating current wedge, play a significant role in the generation of Pi2's observed in the equatorial magnetosphere (Takahashi et al., 1992; Takahashi et al., 1995; Takahashi et al., 1999). A relation between the onset timing of Pi2s and high speed flow in the central plasma sheet termed bursty bulk flows (BBFs) is noted by Shiokawa et al. (1998). Later, Kepko and Kivelson (1999) and Kepko et al. (2001) reported a one-to-one correspondence between low-latitude Pi2s and the temporal variations in the BBFs. These studies suggest that the compression of the inner magnetosphere caused by the BBFs can be the cause for Pi2 oscillations in the inner magnetosphere, indicating that Pi2 pulsations are directly driven by oscillatory external source.

5.1.1.3. Oscillating Substorm Current Wedge

During substorm onset, the magnetic field perturbations at nighttime ground stations can be explained by a simple line current model of substorm current wedge developed by McPherron et al. (1973) and Clauer and McPherron (1974). According to this model, the onset of the expansion phase of the substorm is marked by the disruption of cross-tail currents. A portion of the inner edge of the disrupted tail current is then diverted into the ionosphere as downward FAC in the dawnside and upward FAC in the duskside, which are connected in the auroral ionosphere through westward electrojet currents. Lester et al. (1983) identified that the polarization direction of midlatitude Pi2 pulsations in the nightside has a specific longitudinal pattern, which is well oriented with the FAC geometry of SCW. We use this three-dimensional current geometry of SCW FACs to explain the nightside Pi2 oscillations observed in the three orthogonal magnetic field components at satellite and ground locations.

5.1.2. Magnetic Field Variations Expected From Oscillating SCW Model

Figure 9 demonstrates the nightside view of the possible oscillation of SCW FACs in both NH and SH along with the directions of the associated magnetic field perturbations in the H , D , and Z components observed at ground locations inside the current wedge. Note that these directions of the FACs and the associated magnetic field variations are one phase of the oscillation of the FACs, for which we take the direction same to that of the background SCW.

At longitudes inside the current wedge, which spans several hours in the premidnight to postmidnight LTs, the perturbations in the H component due to both upward and downward FACs will be directed northward in the both hemispheres. This will result in same phase in the H component inside the current wedge. However, the D component will undergo a phase reversal across the central meridian of SCW due to the opposite direction sense of the two contributing FACs in the dawn and dusk LT. In the NH, the D variations on the right side of the central meridian will be directed westward due to downward FAC and that on the

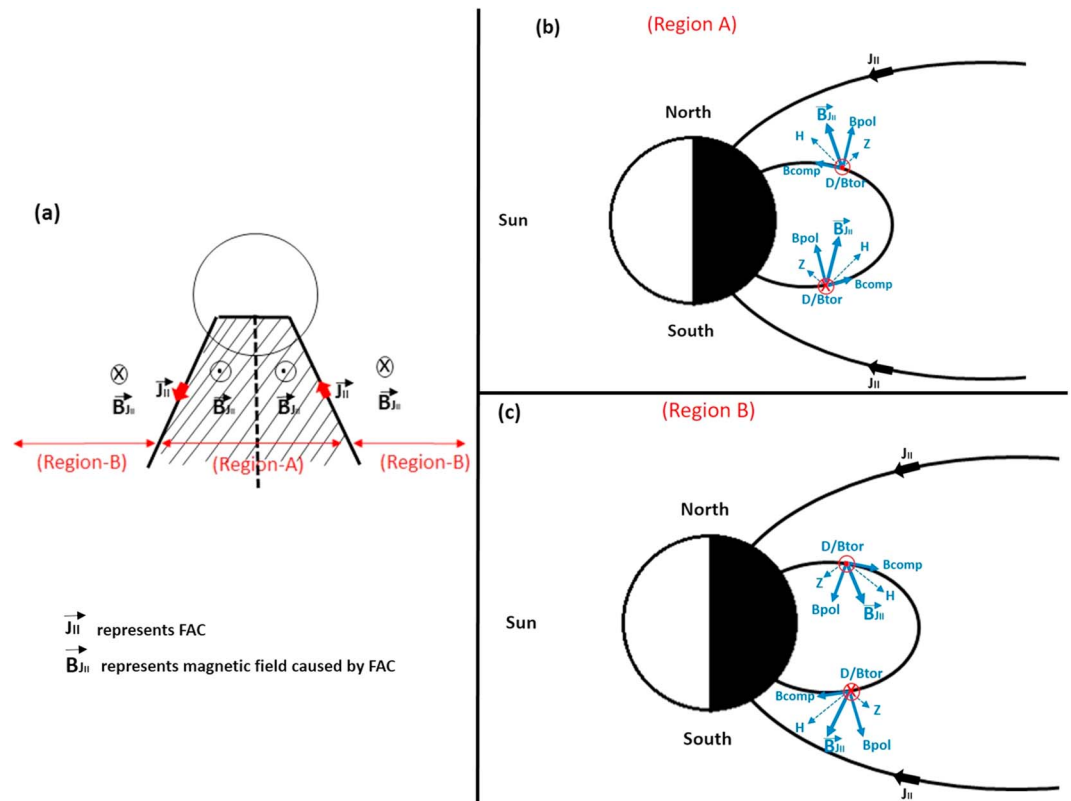


Figure 10. Schematic view of the (a) different regions of substorm current wedge field-aligned currents (FACs), looking from above the current system and the predicted directions of the magnetic field variations in the meridional plane caused by the one phase of oscillating FACs in the Northern Hemisphere and Southern Hemisphere at locations (b) inside and (c) outside the current wedge. The directions of the magnetic field variations are represented in geomagnetic (H , D , and Z) and field aligned (B_{comp} , B_{pol} , and B_{tor}) coordinate systems.

left will be directed eastward due to upward flowing FAC. However, D variations in the SH will be opposite, as the geomagnetically conjugate FACs will produce opposite D variations in the opposite hemisphere. The FAC geometry will therefore result in phase reversal in the D component across the central meridian as well as across the hemispheres. At low-middle latitude locations inside the current wedge, as the magnetic field vector of FAC is inclined above the horizontal plane of the Earth in the NH and below in the SH, FACs can result in Z variations, which are vertically upward (negative Z) in the NH and downward (positive Z) in the SH. This will result in a phase reversal in the Z component across hemispheres. However, inside the current wedge, the direction of Z component will remain constant at each hemisphere.

Figure 10 illustrates the magnetic field variations in the meridional ($H - Z$) plane both inside (Figure 10b) and outside (Figure 10c) the current wedge using a single current wedge FAC in the NH and SH. Please note that we use one phase of the oscillating FAC to discuss the direction of magnetic field components, which will reverse in the other phase of the oscillation. As depicted in Figure 10a, the region inside the current wedge is marked as Region A and that outside is marked as Region B. Here the magnetic field vector resulted by the FAC is denoted as $B_{J_{||}}$, which has a northward component in Region A (inside the current wedge) and a southward component in Region B (outside the current wedge). As mentioned above, $B_{J_{||}}$ is usually inclined from the horizontal plane of the Earth at the low-middle latitude locations. As a result, the magnetic field variations caused by FAC can be observed in both horizontal and vertical directions. The components of $B_{J_{||}}$ represented in both geomagnetic (H , D , and Z) and field-aligned (B_{comp} , B_{tor} , and B_{pol}) coordinates in Region A and Region B are depicted in Figures 10b and 10c. It should be noted that the components H (Z) and B_{comp} (B_{pol}) are separated by the angle of inclination, with D and B_{tor} directed along the same direction.

Figure 10b shows the magnetic field variations caused by a single downward FAC inside the current wedge (Region A) at NH and SH. In Region A, the FAC will cause positive perturbations in the H and B_{comp} (compressional) components at both NH and SH, with H directed toward north and B_{comp} along the direction of

local magnetic field line. The vertical components of $B_{J_{\parallel}}$ (Z and B_{pol}) on the other hand has opposite directions in opposite hemispheres. In the NH, as $B_{J_{\parallel}}$ is tilted above the horizontal plane of the Earth, Z and B_{pol} will be directed vertically outward, resulting in negative perturbations by their definition of direction. In the SH with $B_{J_{\parallel}}$ tilted below the horizontal plane of Earth, Z and B_{pol} will be directed vertically inward, resulting in positive perturbations.

In Region B (Figure 10c), outside the current wedge, as the direction of $B_{J_{\parallel}}$ reverses, the directions of both horizontal and vertical components of $B_{J_{\parallel}}$ will also reverse. H component will be directed southward and B_{comp} component will be directed antiparallel to local magnetic field line, in both the hemispheres resulting in negative perturbations in H and B_{comp} . Vertical components of $B_{J_{\parallel}}$ (Z and B_{pol}) will be directed vertically inward in the NH and outward in the SHs. This shows that the H/B_{comp} and Z/B_{pol} components of $B_{J_{\parallel}}$ will undergo a phase reversal across the FAC, between Region A and Region B. In this field line geometry depicting a single downward FAC, as illustrated in Figures 9 and 10, the D and B_{tor} components will be directed westward in the NH and eastward in the SH. However, these azimuthal variations inside and outside the current wedge due to a single FAC will remain unchanged. It is to be noted again that the directions mentioned here are the initial direction of the oscillations that will reverse after a half wave cycle.

5.1.3. Comparison of Present Observations With Oscillating SCW Model

It was shown by previous researchers that the current wedge spans several hours in LT in the nightside, with center located around premidnight LT (Lester et al., 1983; McPherron et al., 1973). As a result, the downward and upward FACs of SCW can be located symmetrically in the postmidnight to dawn and premidnight to dusk LT sectors, respectively. Also, the location of FACs in LT may vary from event to event depending on the location of the center of the current wedge and its longitudinal extent. It is evident from the above discussion that the H component of oscillating FAC at any location inside the current wedge will be uniformly directed northward (positive) during the first half of the wave cycle resulting in the in-phase oscillations at both NH and SH. As it is reasonable to consider a midnight ground station to be always located within the current wedge, we have compared the phase of different magnetic field components both inside and outside the current wedge with that of midnight ground H (which will have positive perturbations in the initial phase of the oscillation). Different magnetic field components (depicted in Figures 9 and 10) with initial perturbations directed positive will result in the in phase and that directed negative will result in the out of phase with midnight H . The expected phase pattern of different magnetic field components with respect to midnight ground H , explained using the above-discussed SCW model are summarized in Table 3. For the sake of comparison, the observed phase relations of different magnetic field components at satellite and ground with respect to midnight ground H are also indicated in Table 3, within brackets.

The characteristic features of nighttime Pi2 signatures at ground and satellite presented in Figures 6 and Figure 7, respectively, adhere very much to the above-discussed phase pattern of magnetic field components inside the SCW. Our observations of Pi2 signatures in the H component in Figure 6a, showed nearly in-phase oscillations at night hours centered around midnight, which then tend to reverse its phase at LT between premidnight/postmidnight to terminator hours. As downward and upward FACs contribute to northward H inside the current wedge (Figure 10a), one can expect a maximum amplitude of the H component at the center of current wedge, which decreases toward the FAC locations. Our observations of the maximum amplitude (Figure 6b) and in-phase (Figure 6a) oscillations of the H component near midnight hours along with the decreasing tendency in the amplitude and increasing tendency in the phase toward premidnight to terminator hours/postmidnight to terminator hours, follows the direction sense and the amplitude of the H oscillations expected from the current wedge model. It is also obvious from the observations that phase and amplitude of H oscillations are independent of latitude. The compressional oscillations observed by satellite at night (Figure 7a) are also identical to H oscillations at ground. The observation in Figures 6a and 7a also validates our analysis of using the midnight ground H as the reference of the phase relationship, because it always has same phase at both hemispheres with large amplitudes.

The Pi2 oscillations observed in the D components provide more convincing evidence for the FAC geometry (Figure 6c). At LTs between 18 and 0 hr, the D component in the NH and SH oscillate in phase and out of phase, respectively, with midnight H . In the postmidnight sector between 0 and 6 hr, the phase of D is found to reverse in both the hemispheres. The phase relationship of the D component with respect to midnight H is in accordance with the results of (Li et al., 1998; Osaki et al., 1996), who showed that the Pi2 oscillations in the D component undergo a phase reversal across hemispheres and across the Pi2 source longitude. This specific phase pattern in the Pi2 oscillations in the D component follows very well the FAC geometry of SCW

Table 3

Expected Phase Relationship During Nighttime for Different Magnetic Field Components at Topside Ionosphere and Ground With Respect to Midnight Ground H in View of Oscillating Substorm Current Wedge Model^a

Components	Hemisphere	Inside current wedge		Outside current wedge	
		Left of central meridian	Right of central meridian	Left of central meridian	Right of central meridian
H	NH	In phase ($\sim 0^\circ$)	In phase ($\sim 0^\circ$)	Out of phase ($\sim 0^\circ$)	Out of phase ($0-120^\circ$)
	SH	In phase ($\sim 0^\circ$)	In phase ($\sim 0^\circ$)	Out of phase ($\sim 0^\circ$ to -100°)	Out of phase (~ 0 to $\pm 180^\circ$)
D	NH	In phase ($\sim 0^\circ$)	Out of phase ($\sim \pm 180^\circ$)	In phase ($\sim 180^\circ$)	Out of phase ($\sim 0^\circ$)
	SH	Out of phase ($\sim \pm 180^\circ$)	In phase ($\sim 0^\circ$)	Out of phase ($-180-0^\circ$)	In phase ($\sim \pm 180^\circ$)
Z	NH	Out of phase ($\sim 0^\circ, 180^\circ$)	Out of phase ($\sim 0^\circ$)	In phase ($\sim 0^\circ, \pm 180^\circ$)	In phase ($\sim 0^\circ, \pm 180^\circ$)
	SH	In phase ($\pm 180^\circ$)	In phase ($\sim \pm 180^\circ$)	Out of phase ($\sim 0^\circ, \pm 180^\circ$)	Out of phase ($\sim 0^\circ, \pm 180^\circ$)
B_{comp}	NH	In phase ($\sim 0^\circ$)	In phase ($\sim 0^\circ$)	Out of phase (No observation)	Out of phase (No observation)
	SH	In phase ($\sim 0^\circ$)	In phase ($\sim 0^\circ$)	Out of phase (No observation)	Out of phase (No observation)
B_{tor}	NH	In phase ($\sim 0^\circ$)	Out of phase ($\sim 180^\circ$)	In phase (No observation)	Out of phase (No observation)
	SH	Out of phase (No observation)	In phase ($\sim 0^\circ$)	Out of phase (No observation)	In phase (No observation)
B_{pol}	NH	Out of phase ($\sim 180^\circ$)	Out of phase ($\sim 180^\circ$)	In phase (No observation)	In phase (No observation)
	SH	In phase (No observation)	In phase ($\sim 0^\circ$)	Out of phase (No observation)	Out of phase (No observation)

^aThe corresponding observed phase relations are given in brackets. NH = Northern Hemisphere; SH = Southern Hemisphere.

shown in Table 3. The toroidal oscillations at satellite (Figure 7c) observed in the premidnight and postmidnight hours are also found to be in accordance with that of D at this LT sector. The simultaneous observations of Pi2 oscillations in the satellite toroidal and ground D components, which showed phase reversal across hemispheres and also across midnight meridian clearly indicate that both satellite and ground witnessed the oscillations caused by the overhead downward and upward FACs in the dawnside and duskside, respectively.

For locations inside the current wedge, the magnetic field perturbations in the vertical (Z and toroidal) components caused by oscillating FACs are expected to be out of phase in the NH and in phase in the SH, as shown in Table 3. Although coherent Pi2 signatures are observed in the Z component of the magnetic field in Figure 6e, they did not seem to have a systematic phase relation. On the other hand, the poloidal oscillations observed at satellite (Figure 7e) in the premidnight and postmidnight hours showed a systematic phase relation, which is out of phase in the NH and in phase in the SH. This phase relationship observed in the poloidal component is in accordance with that of oscillating FACs for locations inside the current wedge described in Table 3. It is interesting to note that the poloidal oscillations at satellite could reflect the magnetic field signatures of oscillating FACs. However, the ground failed to reproduce the same. This difference in the observations at satellite and ground may be due to the contamination of the ground Pi2 signatures in the Z component due to the secondary magnetic fields caused by the induced currents at ground (Parkinson, 1962). As discussed above, the phase relationships of magnetic field oscillations observed in this study at multipoint ground and satellites at nightside are consistent with the phase relationships expected from the oscillating SCW FACs presented in Table 3.

5.1.4. Discussion Nighttime

Our observations clearly show the existence of Pi2 oscillations in the toroidal component together with the compressional and poloidal components in the topside ionosphere during night hours. These toroidal component in the topside ionosphere is found to have coherent oscillations with the D at ground, with both toroidal and D components following same phase relations. The compressional and poloidal components showed coherent oscillations with ground H , with compressional component showing identical phase relations with H at ground. These observations strongly imply that both ground and satellite witnessed same oscillations above them in the magnetosphere, which are manifested in all the three magnetic field components with little influence of the ionosphere on these oscillations. The coherent Pi2 signatures observed in all the three magnetic field components at satellite and ground also point out the three-dimensional structure of the source field. Hence, our observations from topside ionosphere and ground strongly suggest that the nighttime low-middle latitude Pi2s observed at near Earth locations (i.e., at ground and ionosphere) are the manifestation of the SCW FAC oscillations.

The results of present study is different from that of the previous results by Takahashi et al. (1992, 1995, 1999, 2001, 2011), which proposed cavity oscillations as the source for low-latitude Pi2. This difference in the Pi2 source mechanism could be because of the difference in observation locations. Although our observations are limited to the topside ionosphere, we believe that the contribution of oscillating FAC on low-latitude Pi2 may be less dominant at far-Earth locations, (i.e., at plasmasphere and plasmatrough) compared to that at ground and at LEO satellite altitudes. Near the Earth's surface (i.e., at ground and ionospheric altitudes), the downward and upward FACs are closely located (i.e., the distance between them is less). As the radial distance increases, the downward and upward FACs will be widely separated in space. This may result in a lesser contribution of oscillating FACs in the compressional component in the equatorial plane at magnetospheric altitudes ($L = 6$). Also, the FACs are more spatially localized and closer to the satellite at LEO altitudes compared to that in the magnetosphere. This can also result in the lesser contribution of oscillating FAC on low-latitude Pi2s in the far-Earth locations. A dipolarization event in the near-Earth plasma sheet, will launch different wave modes (compressional and transverse) in the plasma sheet. The compressional wave front propagates Earthward in the equatorial plane and may excite plasmaspheric cavity/virtual resonance. With compressional source region more localized to equatorial plane in the near-Earth plasma sheet, the plasmaspheric cavity/virtual resonance caused by the compressional fast wave modes may have dominant contribution at equatorial magnetosphere rather than the oscillation by the SCW FACs. These are our speculations on why the two different mechanisms (cavity mode and FAC oscillation) can be proposed based on different observations.

The periodicity of Pi2 oscillations is one important parameter one has to consider. The SCW FAC alone cannot explain the Pi2 periodicity. Therefore, it is important to consider a mechanism that generates FAC oscillations as it decides the periodicity of Pi2 oscillations. The cavity oscillation excited by incoming compressional fast-mode waves can get coupled to shear Alfvén mode and may generate a current system similar to SCW FAC. The FACs carried by the Alfvén waves can result in the Pi2 polarization pattern as observed in the present study. In this scenario, the periodicity of the Pi2 oscillations will be decided by the incoming fast-mode waves. Another possibility is the driving by BBFs in the central plasma sheet. BBFs, as they propagate earthward, brake near the tail/dipolar magnetic field boundary and can result in dawnward inertia current. This inertia current, which flows from dusk to dawn, is diverted along the magnetic field line and result/contribute to the formation of SCW, together with flow shear due to the BBFs (Shiokawa et al., 1997). Kepko et al. (2001) have shown that the Pi2 oscillations at low-middle latitudes can be caused by temporal variations in the inertia current (SCW), rather than the Alfvén wave bouncing between both ionospheres along the geomagnetic field. Hence, the periodicities of the oscillating FACs can be related to the time variations in the fast flow braking, which in turn may be controlled by the magnetospheric processes in the geomagnetic tail.

5.2. Daytime Pi2

Although Pi2 is a nighttime phenomenon, its existence in the daytime, low latitudes are known since several decades. One of the earliest reports of Pi2 pulsations in the daytime was by Yanagihara and Shimizu (1966), who found that daytime Pi2s occur in association with its nighttime counterpart. This was later examined and confirmed by many researchers (Sastry et al., 1983; Stuart & Barszczus, 1980; Sutcliffe & Yumoto, 1989; Nosé et al., 2006) using ground observations. However, the existence of daytime Pi2s in the space was puzzling for long time (Han et al., 2004; Sutcliffe & Lühr, 2010). Thomas et al. (2015, 2016) explained the reasons

Table 4

Expected Phase Relationship of H and D Magnetic Field Components at Ground With Respect to Midnight Ground H During Daytime in View of Oscillating Ionospheric Current Model^a

Components	Hemisphere	Prenoon	Postnoon
<i>H</i>	NH	In phase ($\sim 0^\circ$)	In phase ($\sim 0^\circ$)
	SH	In phase ($\sim 0^\circ$)	In phase ($\sim 0^\circ$)
<i>D</i>	NH	In phase ($\sim 0^\circ$)	Out of phase ($\sim 180^\circ$)
	SH	Out of phase ($\sim \pm 180^\circ$)	In phase ($\sim -90^\circ$)

^aThe corresponding observed phase relations are given in brackets. NH = Northern Hemisphere; SH = Southern Hemisphere.

for the ambiguity in detecting the Pi2s by polar orbiting satellites. In the present study, the daytime Pi2 oscillations are investigated using magnetic field measurements from the Swarm satellites simultaneously located in day and night LT sectors together with ground stations. The study is first of its kind with such distinct data set and can therefore provide important information on the source of daytime Pi2 pulsations. It is to be noted that the present study considers only those events for which compressional oscillations observed at both day and night satellite showed coherent (coherence > 0.6) oscillations with midnight ground *H*, with higher amplitudes in the night sector. This confirms that the selected daytime Pi2 oscillations are not Pc pulsations.

Here we have adopted the schematic illustration of the magnetospheric-ionospheric current closure of sub-storm currents demonstrated by Imajo et al. (2017) to explain the daytime Pi2. According to this model, shown in Figure 10 of Imajo et al. (2017), the perturbations related to Pi2 are launched from the magnetosphere to the polar ionosphere via FACs. In addition to the westward electrojets, a portion of the ionospheric currents caused by FACs in the auroral latitudes can flow toward the sunlit dayside, where it may get connected to the meridional ionospheric currents near the terminators (Yoshikawa et al., 2012). The meridional currents that flow toward the equator in the dawnside at both the hemispheres are closed in the dusk terminator via zonal ionospheric currents in the dayside. These meridional ionospheric currents flowing at dawn and dusk terminators can result in the azimuthal *D* variations in the magnetic field at these LTs. As explained by Imajo et al. (2015, 2017), due to the difference in the contributing currents, from FACs on the night-side to the meridional ionospheric currents on the sunlit side of the terminator, the azimuthal component will undergo a phase reversal around dawn and dusk terminators. In the dayside, toward noon, the meridional ionospheric current becomes mostly eastward (zonal), and as a result the magnetic field perturbations will get polarized to northward *H* component. With the opposite direction sense of the meridional currents between the prenoon and postnoon sectors, the azimuthal magnetic field *D* component will undergo a phase reversal near noon meridian as well. Therefore, according to this ionospheric current geometry (Figure 10 of Imajo et al., 2017), the magnetic field perturbations in the dayside will be confined to the horizontal (*H-D*) plane, with magnetic field oscillations polarized to the *D* component near terminator and to *H* near noon. The expected phase relations of *H* and *D* magnetic field components with respect to midnight ground *H* in view of the ionospheric current model are summarized in Table 4. The expected phase relations in the analogous magnetic field components B_{comp} and B_{hor} in the topside ionosphere with respect to underneath ground *H* and *D*, respectively, are presented in Table 5. Please note that, in Tables 4 and 5, the actual phase observations are provided in brackets for the sake of comparison.

The simultaneous observations of Pi2 oscillations in the satellite compressional component at day and night LT reported in this paper provide convincing evidence for the ionospheric current model of daytime Pi2. The compressional oscillations at satellite is found to have opposite phase relation at day and night with compressional component oscillating in phase at night and antiphase at day with midnight ground *H* (Figure 7a). In the daytime, the compressional component is also found to oscillate antiphase with underneath ground *H* (Figure 8a). The antiphase oscillations observed in the daytime satellite compressional and underneath

Table 5

Expected Phase Relationship of Compressional and Toroidal Magnetic Field Components at Topside Ionosphere With Respect to Underneath Ground H and D , Respectively, During Daytime in View of Oscillating Ionospheric Current Model^a

Components	Hemisphere	Prenoon	Postnoon
B_{comp}	NH	Out of phase ($\pm 180^\circ$)	Out of phase ($\pm 180^\circ$)
	SH	Out of phase ($\pm 180^\circ$)	Out of phase ($\pm 180^\circ$)
B_{tor}	NH	Out of phase (No observation)	Out of phase ($\pm 180^\circ$)
	SH	Out of phase (No observation)	Out of phase ($\pm 180^\circ$)

^aThe corresponding observed phase relations are given in brackets. NH = Northern Hemisphere; SH = Southern Hemisphere.

ground H is a clear indication of the role of ionospheric currents in the generation of daytime Pi2s, which will cause opposite magnetic field perturbations above and below the ionosphere.

The dense network of ground station used here enabled to visualize for the first time the phase and amplitude structure of the global Pi2 oscillations in the H and D components. The Pi2 oscillations observed in the D component is found to have specific phase pattern in the day and night LT sectors (Figure 6c). As evident from Figure 6c, in addition to the midnight meridian, the D component is found to have phase reversal at three LT meridians: (1) near dawn terminator around 6 LT, (2) near noon meridian around 12 LT, and (3) near dusk terminator around 18 LT with opposite D oscillations in opposite hemispheres. These phase variations of the D component near dawn/dusk terminators and noon are well in accordance with the ionospheric current model of Imajo et al. (2017), where (1) and (3) can be explained by the meridional currents near the dawn (dusk) terminators, which results in D variations opposite to that of FACs in the postmidnight (premidnight) hours, as shown in Figure 10 of Imajo et al. (2017). Also the phase reversal across the noon meridian (2) can be attributed to the opposite sense of meridional ionospheric currents in the prenoon and postnoon hours. It should be also noted that in the dayside (6–18 LT), the amplitude of the H component showed an increasing trend and the D component showed a decreasing trend toward the noon, which indicates that the Pi2 oscillations are polarized to H component near noon and D component near terminator. The coherent toroidal oscillations observed during daytime were found to be nearly antiphase with underneath ground D (Figure 8b). This again supports the idea of ionospheric currents as the source for daytime Pi2s.

5.3. Terminator Pi2

It was shown by the previous researchers that the phase of the H component at low latitudes does not vary with LT (Imajo et al., 2017; Nosé et al., 2006; Sutcliffe & Yumoto, 1991). However, less investigated is the variation in the phase of the H component near the terminator hours. Although the SCW model predicts a phase reversal in the H component outside the wedge, there were no observations in support of this. The present study demonstrates for the first time that the H component undergo significant phase and amplitude variations near the terminators, with changes more remarkable in the dawn sector.

At locations outside the current wedge, the Pi2 oscillations in the H component can be influenced by both FACs and the meridional ionospheric currents, with FACs causing antiphase oscillations and the meridional ionospheric currents with horizontal inclination causing in-phase oscillations. In the dawn sector, as shown in Figure 10 of Imajo et al. (2017), the little inclination of the meridional currents with horizontal will contribute less to H component, and therefore, the contribution of FAC may dominate. However, in the dusk sector, as the meridional currents are more horizontally inclined, it can result in the oscillations in the H component, which will be opposite to that caused by the FAC outside the current wedge. This indicates that in the dawn sector, the phase of H may be governed mostly by the FAC, whereas in the duskside, the observed phase in H may be the net result of FAC and meridional currents.

It has also to be noticed that, as the SCW itself is centered around premidnight hours, the FACs and the meridional currents may be more closely located in the duskside than in the dawnside. As a result, the phase reversal meridian may be more longitudinally localized and therefore may be less evident at dusk LT sector. Also, at low-latitude ground locations one can consider the effect of the meridional ionospheric currents to be stronger than FACs. The dominance of the meridional current and the longitudinal localization of the phase reversal meridian can together make the change in the phase of H component less evident at dusk LT. However on the dawnside, for events when FAC and equatorward meridional currents are well separated in longitude, the phase reversal in H can be identified with a dense network of ground station distributed in latitude and longitude.

As indicated by Lester et al. (1989), at low latitudes, as the longitudinal span of the SCW gets wider, the polarization pattern breaks down far from the wedge center as the signal gets weak at these latitudes. It is evident from Figure 6a that the H component phase reversal in the dawnside is only recorded by a few stations that are located at relatively higher latitudes. However, a change in phase from $\sim 120^\circ$ – 0° is clearly evident across the dawn terminator. Hence, our observations in the H and D components from ground network together with satellite compressional component strongly suggest that daytime low-latitude Pi2s are the manifestation of ionospheric currents in the E region, which may be caused by the electric fields carried by FACs from the magnetosphere to auroral ionosphere. Investigation of terminator Pi2 using conjugate observations from satellite and ground observations can throw further light on the complex coupling process taking place at these LTs.

6. Conclusion

The present study investigates the Pi2 oscillations using multipoint observations from the Swarm satellites in the topside ionosphere and a dense network of equator to midlatitude ground stations distributed around the globe. The simultaneous observations of Pi2 oscillations in the compressional, toroidal, and poloidal components at satellite and in H , D , and Z components at ground facilitate to obtain a three-dimensional view of Pi2 oscillations at middle and low latitudes. The main outcomes of the study are summarized below.

During nighttime,

1. The H component is found to oscillate mostly in phase with midnight H . However, a change in phase is observed near the postmidnight to dawn hours. The H amplitude showed peak value near premidnight hours and a decreasing trend toward dawn and dusk terminators, with changes remarkable in the dawnside. The change in amplitude and phase of H near terminators indicate the contribution of different Pi2 source at this LT.
2. The compressional component in the topside ionosphere showed in-phase oscillations with midnight H , indicating identical oscillations in the satellite compressional and ground H during nighttime. This fact indicates that the source of the nighttime Pi2 is the current well above the ionosphere, possibly in the magnetosphere or between the magnetosphere and the ionosphere.
3. The D component phase is found to be systematically structured with LT as well as latitude. In the nighttime, D component showed phase reversal across the midnight meridian. The phase of D is found to be opposite at opposite hemispheres, indicating the symmetric nature of the source of Pi2 associated D variations. The amplitude of D component did not show clear variation with LT. However, the D amplitude is found to have larger values at higher latitudes. These facts suggest that the source of the nighttime Pi2 is the oscillation of FACs associated with SCW.
4. The toroidal component at satellite showed identical phase relation with that of D at ground, which again indicate the presence of same oscillations above and below the ionosphere during night and suggest the source well above the ionosphere.
5. Poloidal component at satellite is found to have systematic phase during night with cross phase found to be $\sim 0^\circ$ in the SH and $\sim 180^\circ$ in the NH. This fact is again consistent with the idea that the source of the nighttime Pi2 is the oscillation of SCW FAC. However, the cross phase of the Z component did not show clear phase dependence on LT and latitude.

From these clear Pi2 characteristics observed in different magnetic field components above and below the ionosphere, we conclude that the low- and middle-latitude nighttime Pi2 is caused by oscillating SCW FACs.

During daytime,

1. The H component at ground and compressional component in the topside ionosphere are found to oscillate with opposite phase. This fact indicates that the source of the daytime Pi2 is the current in the ionosphere. The amplitude of H oscillations are found to increase from terminator toward noon, with change more evident between 6 and 12 LT. This fact indicates that the zonal ionospheric current increases toward the noon.
2. Daytime Pi2 signatures observed in the D component, showed clear phase variation with LT and latitude. The phase of D is found to reverse across dawn, noon, and dusk meridians, with opposite hemispheres showing opposite phase. This fact is possibly caused by the effects of nighttime SCW FACs and daytime meridional ionospheric currents. Coherent Pi2 oscillations observed in the satellite toroidal component showed opposite phase with that of D at underneath ground stations. This fact again indicates that the source of the daytime Pi2 is the current in the ionosphere.
3. Poloidal and Z components did not seem to have systematic phase pattern during daytime.

These daytime observations, which showed opposite phase in the compressional and toroidal components at satellite with H and D , respectively, at ground indicate the oscillating ionospheric currents as the source of daytime Pi2s.

Acknowledgments

Authors are grateful to ESA for providing high-quality magnetic field data from Swarm satellites. The Swarm data used here are MAGX_LR_1B and are freely accessible at <http://earth.esa.int/web/guest/swarm/data-access>. The results presented in this paper also rely on 1-s magnetic field data collected at various magnetic observatories. Authors thank the national institutes that support them and INTERMAGNET for promoting high standards of magnetic observatory practice (www.intermagnet.org). Data from the Hermanus (HER) Magnetic observatory are made available through the South African National Space Agency (SANSA). Authors gratefully acknowledge Alma Ata (AAA) magnetic observatory for providing data on request. We thank Dr. Yuki Obana for magnetic field data from Middlemarch (MDM) and Te Wharau (TEW) ground observatories and Research Institute for Sustainable Humanosphere (RISH), Kyoto University, and the National Institute of Aeronautics and Space (LAPAN), Indonesia, for data from Kototabang (KTB). We also thank WDC for geomagnetism, Kyoto (<http://wdc.kugi.kyoto-u.ac.jp/>) for providing AL and Wp indices. G. V. is supported by ISEE International Collaborative Research Program. This research was supported by the JSPS Core-to-Core Program, B. Asia-Africa Science Platforms, and JSPS KAKENHI grants (JP 15H05815 and JP 16H06286).

References

- Allan, W., Menk, F., Fraser, B., Li, Y., & White, S. (1996). Are low-latitude Pi2 pulsations cavity/waveguide modes? *Geophysical Research Letters*, *23*(7), 765–768.
- Allan, W., Poulter, E., & White, S. (1986). Hydromagnetic wave coupling in the magnetosphere–plasma-pause effects on impulse-excited resonances. *Planetary and Space Science*, *34*(12), 1189–1200.
- Balasis, G., Daglis, I. A., Zesta, E., Papadimitriou, C., Georgiou, M., Haugmans, R., & Tsinganos, K. (2012). ULF wave activity during the 2003 Halloween superstorm: Multipoint observations from CHAMP, Cluster and Geotail missions. *Annales Geophysicae*, *30*, 1751–1768. <https://doi.org/10.5194/angeo-30-1751-2012>
- Balasis, G., Papadimitriou, C., Daglis, I. A., & Pilipenko, V. (2015). ULF wave power features in the topside ionosphere revealed by Swarm observations. *Geophysical Research Letters*, *42*, 6922–6930. <https://doi.org/10.1002/2015GL065424>
- Clauer, C. R., & McPherron, R. L. (1974). Mapping the local time-universal time development of magnetospheric substorms using mid-latitude magnetic observations. *Journal of Geophysical Research*, *79*(19), 2811–2820.
- Cummings, W., Barfield, J. N., & Coleman, P. J. (1968). Magnetospheric substorms observed at the synchronous orbit. *Journal of Geophysical Research*, *73*(21), 6687–6698.
- Finlay, C. C., Olsen, N., Kotsiaros, S., Gillet, N., & Tøffner-Clausen, L. (2016). Recent geomagnetic secular variation from swarm and ground observatories as estimated in the CHAOS-6 geomagnetic field model. *Earth, Planets and Space*, *68*(1), 112.
- Finlay, C. C., Olsen, N., & Tøffner-Clausen, L. (2015). DTU candidate field models for IGRF-12 and the CHAOS-5 geomagnetic field model. *Earth, Planets and Space*, *67*(1), 114.
- Fujita, S., Nakata, H., Itonaga, M., Yoshikawa, A., & Mizuta, T. (2002). A numerical simulation of the Pi2 pulsations associated with the substorm current wedge. *Journal of Geophysical Research*, *107*(A3), 1034. <https://doi.org/10.1029/2001JA900137>
- Gelpi, C., Hughes, W., Singer, H., & Lester, M. (1985). Mid-latitude Pi2 polarization pattern and synchronous orbit magnetic activity. *Journal of Geophysical Research*, *90*(A7), 6451–6458.
- Han, D.-S., Iyemori, T., Nosé, M., McCreddie, H., Gao, Y., Yang, F., et al. (2004). A comparative analysis of low-latitude Pi2 pulsations observed by orsted and ground stations. *Journal of Geophysical Research*, *109*, A10209. <https://doi.org/10.1029/2004JA010576>
- Heilig, B., Lühr, H., & Rother, M. (2007). Comprehensive study of ulf upstream waves observed in the topside ionosphere by CHAMP and on the ground. In *Annales geophysicae* (Vol. 25, pp. 737–754).
- Heilig, B., & Sutcliffe, P. R. (2016). Coherence and phase structure of compressional ULF waves at low-Earth orbit observed by the Swarm satellites. *Geophysical Research Letters*, *43*, 945–951. <https://doi.org/10.1002/2015GL067199>
- Imajo, S., Yoshikawa, A., Uozumi, T., Ohtani, S., Nakamizo, A., & Chi, P. (2017). Application of a global magnetospheric-ionospheric current model for dayside and terminator Pi2 pulsations. *Journal of Geophysical Research: Space Physics*, *122*, 8589–8603. <https://doi.org/10.1002/2017JA024246>
- Imajo, S., Yoshikawa, A., Uozumi, T., Ohtani, S., Nakamizo, A., Demberel, S., & Shevtsov, B. M. (2016). Solar terminator effects on middle-to low-latitude Pi2 pulsations. *Earth, Planets and Space*, *68*(1), 137.
- Imajo, S., Yoshikawa, A., Uozumi, T., Ohtani, S., Nakamizo, A., Marshall, R., et al. (2015). Pi2 pulsations observed around the dawn terminator. *Journal of Geophysical Research: Space Physics*, *120*, 2088–2098. <https://doi.org/10.1002/2013JA019691>
- Itonaga, M., & Yoshikawa, A. (1996). The excitation of shear Alfvén wave and the associated modulation of compressional wave in the inner magnetosphere. *Journal of Geomagnetism and Geoelectricity*, *48*(11), 1451–1459.
- Jadhav, G., Rajaram, M., & Rajaram, R. (2001). Modification of daytime compressional waves by the ionosphere: First results from OERSTED. *Geophysical Research Letters*, *28*(1), 103–106.
- Keiling, A., Marghita, O., Vogt, J., Amm, O., Bunescu, C., Constantinescu, V., et al. (2014). Magnetosphere-ionosphere coupling of global Pi2 pulsations. *Journal of Geophysical Research: Space Physics*, *119*, 2717–2739. <https://doi.org/10.1002/2013JA019085>
- Keiling, A., Wygant, J., Cattell, C., Kim, K.-H., Russell, C., Milling, D., et al. (2001). Pi2 pulsations observed with the polar satellite and ground stations: Coupling of trapped and propagating fast mode waves to a midlatitude field line resonance. *Journal of Geophysical Research*, *106*(A11), 25,891–25,904.
- Kepko, L., & Kivelson, M. (1999). Generation of Pi2 pulsations by bursty bulk flows. *Journal of Geophysical Research*, *104*(A11), 25,021–25,034.

- Kepko, L., Kivelson, M., & Yumoto, K. (2001). Flow bursts, braking, and Pi2 pulsations. *Journal of Geophysical Research*, *106*(A2), 1903–1915.
- Kikuchi, T., & Araki, T. (1979). Horizontal transmission of the polar electric field to the equator. *Journal of Atmospheric and Terrestrial Physics*, *41*(9), 927–936.
- Kivelson, M. G., & Southwood, D. J. (1986). Coupling of global magnetospheric mhd eigenmodes to field line resonances. *Journal of Geophysical Research*, *91*(A4), 4345–4351.
- Kivelson, M. G., & Southwood, D. J. (1988). Hydromagnetic waves and the ionosphere. *Geophysical Research Letters*, *15*(11), 1271–1274.
- Lee, D.-H. (1996). Dynamics of MHD wave propagation in the low-latitude magnetosphere. *Journal of Geophysical Research*, *101*(A7), 15,371–15,386.
- Lester, M., Hughes, J. W., & Singer, H. J. (1983). Polarization patterns of Pi2 magnetic pulsations and the substorm current wedge. *Journal of Geophysical Research*, *88*(A10), 7958–7966.
- Lester, M., Hughes, W. J., & Singer, H. J. (1984). Longitudinal structure in Pi2 pulsations and the substorm current wedge. *Journal of Geophysical Research*, *89*(A7), 5489–5494.
- Lester, M., Singer, H. J., Smits, D. P., & Hughes, W. Jeffrey (1989). Pi2 pulsations and the substorm current wedge: Low-latitude polarization. *Journal of Geophysical Research*, *94*(A12), 17,133–17,141.
- Li, Y., Fraser, B., Menk, F., Webster, D., & Yumoto, K. (1998). Properties and sources of low and very low latitude Pi2 pulsations. *Journal of Geophysical Research*, *103*(A2), 2343–2358.
- Lin, C., Lee, L., & Sun, Y. (1991). Observations of Pi2 pulsations at a very low latitude ($l = 1.06$) station and magnetospheric cavity resonances. *Journal of Geophysical Research*, *96*(A12), 21,105–21,113.
- McPherron, R. L., Russell, C., & Aubry, M. (1973). Satellite studies of magnetospheric substorms on August 15, 1968: 9. Phenomenological model for substorms. *Journal of Geophysical Research*, *78*(16), 3131–3149.
- Nishimura, Y., Lyons, L., Kikuchi, T., Angelopoulos, V., Donovan, E., Mende, S., et al. (2012). Formation of substorm Pi2: A coherent response to auroral streamers and currents. *Journal of Geophysical Research*, *117*, A09218. <https://doi.org/10.1029/2012JA017889>
- Nose, M. (2010). Excitation mechanism of low-latitude Pi2 pulsations: Cavity mode resonance or bbf-driven process? *Journal of Geophysical Research*, *115*, A07221. <https://doi.org/10.1029/2009JA015205>
- Nose, M., Iyemori, T., Takeda, M., Toh, H., Ookawa, T., Cifuentes-Nava, G., et al. (2009). New substorm index derived from high-resolution geomagnetic field data at low latitude and its comparison with AE and ASY indices. In *Proceedings of XIIIth IAGA Workshop on Geomagnetic Observatory Instruments, Data Acquisition, and Processing*, U.S. Geological Survey Open File Report (Vol. 2009–1226, pp. 202–207). U.S. Geological Survey, Reston, VA.
- Nosé, M., Iyemori, T., Wang, L., Hitchman, A., Matzka, J., Feller, M., et al. (2012). Wp index: A new substorm index derived from high-resolution geomagnetic field data at low latitude. *Space Weather*, *10*, S08002. <https://doi.org/10.1029/2012SW000785>
- Nosé, M., Liou, K., & Sutcliffe, P. (2006). Longitudinal dependence of characteristics of low-latitude Pi2 pulsations observed at Kakioka and Hermanus. *Earth, Planets and Space*, *58*(6), 775–783.
- Nosé, M., Takahashi, K., Uozumi, T., Yumoto, K., Miyoshi, Y., Morioka, A., et al. (2003). Multipoint observations of a Pi2 pulsation on morningside: The 20 September 1995 event. *Journal of Geophysical Research*, *108*(A5), 1219. <https://doi.org/10.1029/2002JA009747>
- Osaki, H., Takahashi, K., Fukunishi, H., Nagatsuma, T., Oya, H., Matsuoka, A., & Milling, D. K. (1998). Pi2 pulsations observed from the Akebono satellite in the plasmasphere. *Journal of Geophysical Research*, *103*(A8), 17,605–17,615.
- Osaki, H., Yumoto, K., Fukao, K., Shiokawa, K., Menk, F. W., & Fraser, B. J. (1996). Characteristics of low-latitude Pi2 pulsations along the 210° magnetic meridian. *Journal of Geomagnetism and Geoelectricity*, *48*(11), 1421–1430.
- Papadimitriou, C., Balasis, G., Daglis, I. A., & Giannakis, O. (2018). An initial ulf wave index derived from 2 years of Swarm observations. *Annales Geophysicae*, *36*, 287–299. Copernicus GmbH.
- Parkinson, W. (1962). The influence of continents and oceans on geomagnetic variations. *Geophysical Journal International*, *6*(4), 441–449.
- Saito, T. (1961). Oscillation of geomagnetic field with the progress of pt-type pulsation. Science Reports of the Tohoku University 5th Ser. Geophysics, *13*(2).
- Saito, T., & Matsushita, S. (1968). Solar cycle effects on geomagnetic Pi2 pulsations. *Journal of Geophysical Research*, *73*(1), 267–286.
- Samson, J., Harrold, B., & Yeung, K. (1985). Characteristic time constants and velocities of mid-latitude Pi2's. *Journal of Geophysical Research*, *90*(A4), 3448–3456.
- Sastry, T., Sarma, Y., Sarma, S., & Sanker Narayan, P. (1983). Day-time Pi pulsations at equatorial latitudes. *Journal of Atmospheric and Terrestrial physics*, *45*, 733–741.
- Shinohara, M., Yumoto, K., Yoshikawa, A., Saka, O., Solov'ev, S., Vershinin, E., et al. (1997). Wave characteristics of daytime and nighttime Pi2 pulsations at the equatorial and low latitudes. *Geophysical Research Letters*, *24*(18), 2279–2282.
- Shiokawa, K., Baumjohann, W., & Haerendel, G. (1997). Braking of high-speed flows in the near-Earth tail. *Geophysical Research Letters*, *24*(10), 1179–1182.
- Shiokawa, K., Baumjohann, W., Haerendel, G., Paschmann, G., Fennell, J., Friis-Christensen, E., et al. (1998). High-speed ion flow, substorm current wedge, and multiple Pi2 pulsations. *Journal of Geophysical Research*, *103*(A3), 4491–4507.
- Southwood, D. (1974). Some features of field line resonances in the magnetosphere. *Planetary and Space Science*, *22*(3), 483–491.
- Stuart, W., & Barszczus, H. G. (1980). Pi's observed in the daylight hemisphere at low latitudes. *Journal of Atmospheric and Terrestrial Physics*, *42*(5), 487–497.
- Sutcliffe, P., & Lühr, H. (2003). A comparison of Pi2 pulsations observed by CHAMP in low Earth orbit and on the ground at low latitudes. *Geophysical Research Letters*, *30*(21), 2105. <https://doi.org/10.1029/2003GL018270>
- Sutcliffe, P., & Lühr, H. (2010). A search for dayside geomagnetic Pi2 pulsations in the CHAMP low-Earth-orbit data. *Journal of Geophysical Research*, *115*, A05205. <https://doi.org/10.1029/2009JA014757>
- Sutcliffe, P. R., & Yumoto, K. (1989). Dayside Pi2 pulsations at low latitudes. *Geophysical Research Letters*, *16*(8), 887–890.
- Sutcliffe, P. R., & Yumoto, K. (1991). On the cavity mode nature of low-latitude Pi2 pulsations. *Journal of Geophysical Research*, *96*(A2), 1543–1551.
- Takahashi, K., Anderson, B. J., & Yumoto, K. (1999). Upper atmosphere research satellite observation of a Pi2 pulsation. *Journal of Geophysical Research*, *104*(A11), 25,035–25,045.
- Takahashi, K., Hughes, W., Anderson, R., & Solov'ev, S. (1999). Crres satellite observations associated with low-latitude Pi2 pulsations. *Journal of Geophysical Research*, *104*(A8), 17,431–17,440.
- Takahashi, K., Ohtani, S.-I., & Anderson, B. J. (1995). Statistical analysis of Pi2 pulsations observed by the AMPTE CCE spacecraft in the inner magnetosphere. *Journal of Geophysical Research*, *100*(A11), 21,929–21,941.
- Takahashi, K., Ohtani, S.-I., Hughes, W. J., & Anderson, R. R. (2001). Crres observation of Pi2 pulsations: Wave mode inside and outside the plasmasphere. *Journal of Geophysical Research*, *106*(A8), 15,567–15,581.

- Takahashi, K., Ohtani, Shin-ichi, & Yumoto, K. (1992). AMPTE CCE observations of Pi2 pulsations in the inner magnetosphere. *Geophysical Research Letters*, *19*(14), 1447–1450.
- Takahashi, K., Zanetti, L., Lopez, R., McEntire, R., Potemra, T., & Yumoto, K. (1987). Disruption of the magnetotail current sheet observed by AMPTE/CCE. *Geophysical Research Letters*, *14*(10), 1019–1022.
- Teramoto, M., Takahashi, K., Nosé, M., Lee, D.-H., & Sutcliffe, P. (2011). Pi2 pulsations in the inner magnetosphere simultaneously observed by the active magnetospheric particle tracer explorers/charge composition explorer and dynamics Explorer 1 satellites. *Journal of Geophysical Research*, *116*, A07225. <https://doi.org/10.1029/2010JA016199>
- Thomas, N., Vichare, G., & Sinha, A. (2016). Spatial frequencies associated with the latitudinal structures of ionospheric currents seen by CHAMP satellite. *Astrophysics and Space Science*, *361*(7), 205.
- Thomas, N., Vichare, G., Sinha, A., & Rawat, R. (2015). Low-latitude Pi2 oscillations observed by polar low Earth orbiting satellite. *Journal of Geophysical Research: Space Physics*, *120*, 7838–7856. <https://doi.org/10.1002/2014JA020958>
- Vellante, M., Lühr, H., Zhang, T., Wertzgerom, V., Villante, U., De Lauretis, M., et al. (2004). Ground/satellite signatures of field line resonance: A test of theoretical predictions. *Journal of Geophysical Research*, *109*, A06210. <https://doi.org/10.1029/2004JA010392>
- Yanagihara, K., & Shimizu, N. (1966). Equatorial enhancement of micropulsation Pi2. *Mem. Kakioka Magn. Obs.*, *12*, 57–63.
- Yeoman, T., & Orr, D. (1989). Phase and spectral power of mid-latitude Pi2 pulsations: Evidence for a plasmaspheric cavity resonance. *Planetary and Space Science*, *37*(11), 1367–1383.
- Yoshikawa, A., Ohtani, S., Nakamizo, A., Uozumi, T., & Tanaka, Y. (2012). Formation of Cowling channel from polar to equatorial ionosphere. in *Agu fall meeting abstracts*.
- Yumoto, K. (1990). Evidences of magnetospheric cavity Pi2 waves. *Journal of Geomagnetism and Geoelectricity*, *42*(11), 1281–1290.
- Yumoto, K., Group, C., et al. (2001). Characteristics of Pi2 magnetic pulsations observed at the CPMN stations. *Earth, Planets and Space*, *53*(10), 981–992.